



Intercomparing different devices for the investigation of ice nucleating particles using Snomax[®] as test substance

H. Wex¹, S. Augustin-Bauditz¹, Y. Boose², C. Budke³, J. Curtius⁴, K. Diehl⁵, A. Dreyer^{3,*}, F. Frank⁴, S. Hartmann¹, N. Hiranuma⁶, E. Jantsch^{3,5}, Z. A. Kanji², A. Kiselev⁶, T. Koop³, O. Möhler⁶, D. Niedermeier^{1,**}, B. Nillius^{4,***}, M. Rösch¹, D. Rose⁴, C. Schmidt⁷, I. Steinke⁶, and F. Stratmann¹

¹Experimental Aerosol and Cloud Microphysics, Leibniz Institute for Tropospheric Research (TROPOS), Leipzig, Germany

²Institute for Atmospheric and Climate Science, ETH Zürich, Zürich, Switzerland

³Faculty of Chemistry, Bielefeld University, Bielefeld, Germany

⁴Institute for Atmospheric and Environmental Sciences, Goethe University of Frankfurt, Frankfurt am Main, Germany

⁵Institute of Atmospheric Physics, University of Mainz, Mainz, Germany

⁶Institute for Meteorology and Climate Research, Karlsruhe Institute of Technology (KIT), Karlsruhe, Germany

⁷Institute for Environmental Physics, University of Heidelberg, Heidelberg, Germany

* now at: Institute Advanced Ceramics, Hamburg University of Technology (TUHH), Hamburg, Germany

** now at: Michigan Technological University, Houghton, MI, USA

*** now at: Max Planck Institute for Chemistry, Multiphase Chemistry Department, Mainz, Germany

Correspondence to: H. Wex (wex@tropos.de)

Received: 22 August 2014 – Published in Atmos. Chem. Phys. Discuss.: 1 September 2014

Revised: 17 December 2014 – Accepted: 20 December 2014 – Published: 10 February 2015

Abstract. Seven different instruments and measurement methods were used to examine the immersion freezing of bacterial ice nuclei from Snomax[®] (hereafter Snomax), a product containing ice-active protein complexes from non-viable *Pseudomonas syringae* bacteria. The experimental conditions were kept as similar as possible for the different measurements. Of the participating instruments, some examined droplets which had been made from suspensions directly, and the others examined droplets activated on previously generated Snomax particles, with particle diameters of mostly a few hundred nanometers and up to a few micrometers in some cases. Data were obtained in the temperature range from -2 to -38 °C, and it was found that all ice-active protein complexes were already activated above -12 °C. Droplets with different Snomax mass concentrations covering 10 orders of magnitude were examined. Some instruments had very short ice nucleation times down to below 1 s, while others had comparably slow cooling rates around 1 K min^{-1} . Displaying data from the different instruments in terms of numbers of ice-active protein complexes per dry mass of Snomax, n_m , showed that within their uncertainty, the data agree well with each other as well as to

previously reported literature results. Two parameterizations were taken from literature for a direct comparison to our results, and these were a time-dependent approach based on a contact angle distribution (Niedermeier et al., 2014) and a modification of the parameterization presented in Hartmann et al. (2013) representing a time-independent approach. The agreement between these and the measured data were good; i.e., they agreed within a temperature range of 0.6 K or equivalently a range in n_m of a factor of 2. From the results presented herein, we propose that Snomax, at least when carefully shared and prepared, is a suitable material to test and compare different instruments for their accuracy of measuring immersion freezing.

1 Introduction

In the Earth's atmosphere, different types of clouds exist: warm clouds contain only liquid droplets, cirrus clouds consist solely of ice crystals, and mixed-phase clouds contain both liquid droplets and ice crystals. Ice formation can occur by homogenous freezing of cloud droplets at tempera-

tures below about -38°C , or by heterogeneous ice nucleation processes. In the latter case, a particular aerosol particle, called an ice nucleating particle (INP), induces the ice nucleation, which can occur at all temperatures below 0°C . Immersion freezing is one of the heterogeneous freezing processes, where an INP immersed in a supercooled cloud droplet induces ice nucleation. For mixed-phase clouds, this might be one of the most important freezing process, if not the most important one, as suggested e.g., by Ansmann et al. (2009) and Murray et al. (2012). Below -38°C , homogeneous freezing can take place. Thus, mixed-phase clouds, which are most important for the generation of precipitation outside the tropics, tend to occur at $T > -38^{\circ}\text{C}$. Cirrus clouds found at $T < -38^{\circ}\text{C}$ are generally assumed to have formed by homogeneous freezing; i.e., for cirrus clouds it is thought that homogeneous freezing is the most important mechanism to nucleate ice. However, it was recently suggested by Cziczo et al. (2013) that heterogeneous freezing might be the dominant ice formation mechanism for convective outflow and synoptically formed cirrus in the Northern Hemisphere.

In general, the initiation of ice in clouds, i.e., the ice nucleation process, has to be investigated if we want to understand and describe the formation of precipitation as well as cloud radiative properties, e.g., in weather and climate models. It should also be mentioned that ice multiplication processes (e.g., Hallett and Mossop, 1974) might play an important role for the overall ice content in clouds, too. But even our understanding of ice nucleation in clouds is still limited. DeMott et al. (2011) showed, that a scatter of up to 2 orders of magnitude in measured ice fractions was obtained for Saharan dust samples, when results from different instruments which measured ice nucleation were compared. Mineral dust is considered to contribute a large fraction or even the majority of INPs worldwide (Murray et al., 2012), and K-feldspar was recently reported by Atkinson et al. (2013) to be the most ice nucleation effective mineral dust compound found so far. However, these INPs can only explain ice nucleation in the temperature range below about -15°C , while in atmospheric clouds ice is often observed already at higher temperatures (e.g., Bühl et al., 2013). The presence of biological particles might contribute to the observed high temperatures for ice formation in clouds (Schnell and Vali, 1976; Szyrmer and Zawadzki, 1997; Murray et al., 2012), and recently it was found that in soil dust, biological components on the dust particles enhanced or even determined the particles' ability to nucleate ice (Conen et al., 2011; O'Sullivan et al., 2014; Tobo et al., 2014).

The ice nucleation ability of biological material has been found to originate in ice nucleation active macromolecules (INM) such as some polysaccharides for pollen (Pummer et al., 2012; Augustin et al., 2013) and proteinaceous INM for fungi (Hasegawa et al., 1994; Fröhlich-Nowoisky et al., 2014) and bacteria (e.g., Hartmann et al., 2013, and references therein). Both Augustin et al. (2013) and Hartmann

et al. (2013) were able to determine the ice nucleation ability of single INM for birch pollen and Snomax, respectively. While the discovery of INM active in pollen and fungi was made recently or was only recently intensified again (Pummer et al., 2012; Fröhlich-Nowoisky et al., 2014, respectively), it has long been known that protein complexes are responsible for the ice activity in bacteria. Much research has been done on the latter topic, and the literature cited in the following paragraph is only a small selection of what can be found.

Already Maki et al. (1974) and Green and Warren (1985) described that several bacteria occurring in the atmosphere, among them *Pseudomonas syringae*, can induce heterogeneous freezing at comparatively high temperatures, with freezing sometimes setting in already at about -2°C . Orser et al. (1985) described a gene which produces proteins located in the outer cell membrane which are responsible for the ice nucleation. This gene is highly homologous in all ice-active bacteria. A single ice-active protein was estimated to have a mass of about 150 kDa and to induce freezing at -12 to -13°C (Wolber et al., 1986; Govindarajan and Lindow, 1988). However, the ice-active proteins show a tendency to aggregate, forming protein complexes (e.g., Govindarajan and Lindow, 1988; Southworth et al., 1988; Garnham et al., 2011). It was found for *P. syringae*, that ice nucleation can be induced in the temperature range from about -7 to -10°C . The respective type of protein complexes active in this temperature region was called group III or class C, and it was found that they occurred in about "1 of 300 cells" to "almost all cells" of *P. syringae* cultures (Yankofsky et al. (1981) and Turner et al. (1990), respectively). Responsible for group III ice nucleation behavior are protein complexes of at least two up to a few single ice-active proteins with diameters of a few nanometers. Much more rarely, bacterial cells are observed which induce freezing already at temperatures around -2 to -4.5°C (group I or class A behavior) and around -4.5 to -7°C (group II or class B behavior), where the characterizations in groups is given in Yankofsky et al. (1981) and the one in classes in Turner et al. (1990), both giving slightly different temperature ranges. Different publications give the fraction of cells on which these more ice-active cells occur with 1 in 10^4 to 1 in 10^7 (Yankofsky et al., 1981; Govindarajan and Lindow, 1988; Cochet and Widehem, 2000), associated with much larger protein complexes, containing at least 50 proteins (Govindarajan and Lindow, 1988; Southworth et al., 1988) which corresponds to sizes of roughly some 10 nanometers.

These early findings are in agreement with a recent study by Hartmann et al. (2013), who examined immersion freezing induced by non-viable *P. syringae* present in Snomax. Examined droplets contained single or at most a few of the small protein complexes responsible for the observed group III freezing behavior. Freezing was mostly induced at temperatures from -7 to -10°C , and below -12°C no additional freezing was observed. Snomax is a commercially

available material for artificial snow production and contains non-viable *P. syringae* bacteria and their fragments, i.e., cell constituents and fragments of the cell membrane with or without attached ice-active protein complex, remnants of the nutrition medium used for bacterial cultivation, and some other unknown byproducts. It has been used in the past as surrogate for living bacteria (Wood et al., 2002; Möhler et al., 2008).

Within the research unit INUIT (Ice Nuclei research UnIT, FOR 1525), which is funded by DFG (Deutsche Forschungsgemeinschaft), we did an intercomparison, comparing immersion freezing measured by a suite of different techniques. We examined different test substances. In order to minimize experimental biases in measured data, we shared the same samples and the same particle/droplet production techniques as far as possible while exploring a wide range of experimental conditions concerning particle sizes, droplet concentrations and temperatures. We included mineral dust samples and a biological sample, namely Snomax, in the INUIT comparisons. Results for the former will be presented in separate papers of the same special issue, while the results from the respective comparison for the biological sample will form the focus of this paper.

We present immersion freezing measurements for Snomax, made with seven different instruments in the framework of INUIT. Different Snomax concentrations in the examined droplets are covered, ranging from 6×10^{-12} to 1×10^{-2} mg per droplet. Also, different ice nucleation times were employed, ranging from cooling rates of 1 K min^{-1} to short residence times of below 1 s at a given ice nucleation temperature. Two basically different types of measurement methods were included. Some studies examined droplets which had been generated from Snomax suspensions directly. Others generated dry aerosol particles from Snomax suspensions to enable a size selection and then immersed each of these particles in a droplet. These droplets were then examined with respect to their freezing behavior. In the following, measurement methods and the modeling approach chosen for the data evaluation are briefly discussed, before the results are described in Sect. 4.

2 Measurement methods

In this study, we present a comparison between results obtained from different measurement methods for immersion freezing induced by Snomax. The following seven different instruments are included in the comparison (given in alphabetical order): an acoustic levitator (abbreviated AL herein), AIDA (Aerosol Interaction and Dynamics in the Atmosphere) cloud simulation chamber, BINARY (Bielefeld Ice Nucleation ARraY), FINCH (Fast Ice Nucleus Chamber), LACIS (Leipzig Aerosol Cloud Interaction Simulator), the Mainz vertical wind tunnel (abbreviated WT herein) and PINC (Portable Ice Nucleation Chamber). A more detailed

description of the instrumentation and measurement methods can be found in Appendix A, together with the respective citations of the relevant literature.

Snomax from the same batch was used for all measurements unless mentioned explicitly. It was obtained from SMI Snow Makers AG, Switzerland and distributed to all participating groups. Care was taken to keep the sample frozen at all times, besides short (hour long) breaks during transport by mail from the company to Leipzig and from Leipzig to the INUIT partners. For the latter the Snomax was sent in cooled thermal boxes with thermal insulation.

The measurement methods used by the different instruments within this study can be grouped in two subgroups. On the one hand, there are measurement devices that examined droplets generated directly from suspensions, which are referred to as suspension methods in this study. These include AL, BINARY and WL. The second group consists of AIDA, FINCH, LACIS and PINC, which generally examined droplets activated on size-selected Snomax particles, and in which also some AIDA measurements using polydisperse Snomax aerosol were included. This group of instruments will be referred to as particle methods herein. Important parameters for each method are given in the following two paragraphs and also in Table 1.

Droplets examined with the AL, BINARY and the WT had diameters of 2.0 mm (= 4.2 μL), 1.24 mm (= 1.0 μL) and 0.76 mm (= 0.23 μL), respectively. The suspensions from which the droplets were made contained ultra-pure water and Snomax in defined concentrations. Altogether, examined concentrations ranged from 10^{-8} to 10 mg mL^{-1} , covering 9 orders of magnitude. Figure 1 shows the ranges of Snomax mass per droplet which were used for measurements by the different instruments, while the concentrations of Snomax in the suspensions used to generate the droplet are shown in the legends of Figs. 5 and 6.

At each droplet concentration, a total droplet number of 100 droplets was examined with the AL, and either 144 or 180 droplets were examined in the case of BINARY, while 50 droplets were examined at each concentration and at each temperature by the WT. For the AL, ice nucleation time depended on temperature (see Appendix A1) and the maximum time the droplets spent in the instrument was 10 to 20 s. BINARY was operated at a cooling rate of 1 K min^{-1} . Data reported for WT are integrated ice fractions which were obtained 30 s after the droplets were injected into the instrument, while the instrument remained at a fixed temperature.

For measurements with instruments belonging to the particle methods (AIDA, FINCH, LACIS and PINC), suspensions were used to generate dry particles. These particles were mostly in the sub-micron size range and generated by atomization and subsequent drying in a diffusion dryer. For polydisperse AIDA measurements, particles in the size range above $1 \mu\text{m}$ were also present, as the suspensions were sprayed into the AIDA chamber directly. For sub-micron particles, the particle production was similar to that described in

Table 1. Experimental details for the different measurement techniques/instruments.

Methods examining droplets made directly from suspensions:			
	droplet diameter	number of droplets examined ^{a,b}	cooling rate or ice nucleation time
AL	2.00 mm	100 ^a	temperature dependent, see Appendix A1
BINARY	1.24 mm	144 or 180 ^a	1 K min ⁻¹
WT	0.76 mm	50 ^b	30 s
Methods examining droplets activated on aerosol particles:			
	particle diameter	number of droplets examined ^{a,b}	cooling rate or ice nucleation time
AIDA	200 to 600 nm size-selected, and polydisperse ^c	~ 1000 to 10 000 ^b	~ 1 to 3 K min ⁻¹
FINCH	900 nm	> 2400 ^b	~ 1 s
LACIS	500, 650 and 800 nm	≥ 2000 ^b	≈ 0.2 s at $T < -12$ °C up to 1.6 s at colder T
PINC	500 nm	500 to 3000 ^b	5 s

^a Indicates per concentration, ^b per data point. ^c Polydisperse experiments included also particles < 200 nm.

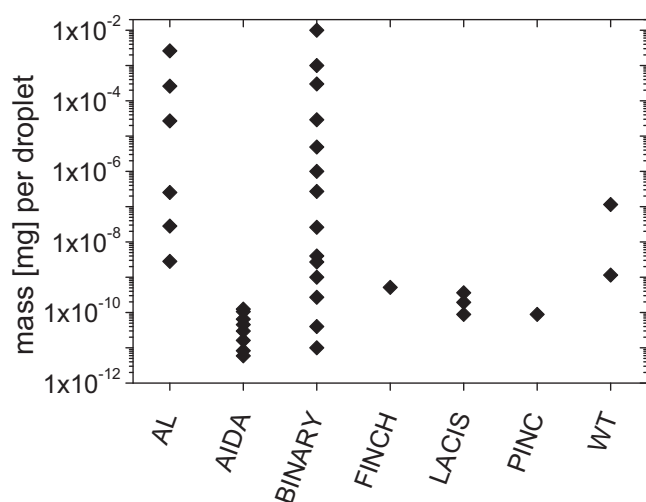


Figure 1. Snomax mass per droplet examined by the different instruments. For AL, BINARY, and WT values follow directly from the Snomax concentration in the suspensions used to produce the droplets, and from the respective droplet size. For AIDA, FINCH, LACIS, and PINC masses were derived using Eq. (2).

detail in Hartmann et al. (2013). All groups used the same atomizer (unless explicitly mentioned), which was sent around within the INUIT community. It was comparable to an atomizer available from TSI (Constant Output Atomizer, Model 3076), but differed in that the outlet for the droplets was at the location of the impaction plate, opposite of the nozzle. In the atomizer, compressed air expands through an orifice, forming a high velocity jet, which then draws liquid into the region of the jet and atomizes it, i.e., forms droplets (see the

instruction manual for TSI Model 3076). The suspensions used in the atomizer had a concentration of 5 g L^{-1} (unless a differing value is given). The droplets generated by the atomizer were dried in diffusion dryers. Subsequently, a DMA (Differential Mobility Analyzer) was used to select a particle size, and the size-selected dry particles were then fed into the instruments (i.e., into AIDA, FINCH, LACIS and PINC). When needed, the particle flow was diluted with dry, particle-free air to reduce the particle number concentration. In all of these instruments particles are activated to droplets which then can freeze upon further cooling.

As for the suspension methods, in the following we give the number of droplets which were examined by the different particle methods, together with the ice nucleation times or cooling rates. These values are also summarized in Table 1. In AIDA, roughly 1000 to 10 000 droplets were counted for each data point; i.e., this is the respective total number of droplets analyzed by the WELAS WhitE-Light Aerosol Spectrometer during a 10 s measurement period. In LACIS, for each separate measurement at each temperature at least 2000 droplets (unfrozen or frozen) were counted; for PINC there were roughly 500 to 3000, and there were at least 2400 in FINCH. In AIDA, cooling rates used to obtain the data presented herein ranged roughly from $1/50$ to $1/20 \text{ K s}^{-1}$ (i.e., approx. 1 to 3 K min^{-1}). Ice nucleation times in the cooled sections in FINCH, LACIS and PINC were $\sim 1 \text{ s}$, $< 1 \text{ s}$ (temperature dependent) and 5 s , respectively.

3 Data analysis

For the presentation of the data in this study, a singular, time independent description was chosen. Hartmann et al.

(2013) derived nucleation rates for the immersion freezing of group III protein complexes in Snomax (thus for *P. syringae*), i.e., for those protein complexes which become ice-active at roughly -7°C . Results in Hartmann et al. (2013) were found to agree with other studies referenced therein, showing that nucleation rates increase steeply over a narrow temperature range. This indicates that the group III protein complexes responsible for inducing the observed ice nucleation are all comparably similar in their ice nucleation ability. Furthermore, it was recently shown that ice nucleation by Snomax shows only a very small time dependence at cooling rates comparable to the current intercomparison (Budke and Koop, 2015), and hence a time-independent treatment of the freezing process seems justifiable. It was clearly shown in Hartmann et al. (2013), that the number of ice nucleation active macromolecules (INM) (i.e., the protein complexes) scaled with the volume of the examined particles, and therefore also with the mass of Snomax present in a droplet. Therefore, in the study presented here, the ice nucleation ability will be expressed per unit mass of Snomax. For similar cases, the following description for the frozen fractions f_{ice} (i.e., the number of frozen droplets divided by the total number of examined droplets) observed for immersion freezing of droplets containing biological material was already introduced by Vali (1971) and again recommended in Murray et al. (2012):

$$f_{\text{ice}}(T) = 1 - \exp(-n_{\text{m}}(T) \cdot C_{\text{m}} \cdot V_{\text{d}}) \quad (1)$$

$n_{\text{m}}(T)$ is the number of INM per unit of dry Snomax mass, C_{m} is the mass concentration of Snomax in the examined droplets and V_{d} is the droplet volume and T the temperature in $^{\circ}\text{C}$. Equation (1) can be used directly for the determination of n_{m} for those measurements, in which droplets of a known concentration are examined, i.e., in our study the suspension methods AL, BINARY, and the WT. For each suspension method, the examined droplets all had an identical size, and during each individual experiment, all droplets had the same Snomax concentration (and different concentrations in different experimental runs). Moreover, as immersion freezing can be assumed to be droplet-volume independent, it ultimately is only necessary to know how many INM were present in a droplet initially. If, in one of the suspension methods, a droplet were to change its size (and hence concentration) due to evaporation or additional condensation, the number of INM present in a droplet would not change. And therefore, the ice nucleation behavior of a droplet would not be affected. This, however, holds only as long as the droplet would not evaporate so much that a freezing point depression due to increased solute concentration started to influence the ice nucleation process (Koop and Zobrist, 2009; Attard et al., 2012).

For the particle methods, neither the exact droplet size was known at the time at which ice nucleation is induced, nor the Snomax concentration in the droplet. But as particles used were either size-selected, or the particle size distribution was

measured, the diameter of the examined particles was known (d_{p}). Snomax particles were generated from suspensions. In Sect. 4.1 we will show that the majority of cell fragments contained in the generated particles were in a size range below 250 nm, together with soluble material. Therefore, it can be assumed that the particles that were examined in this study were spherical. Together with the Snomax density (ρ , see also Sect. 4.1), the mass of Snomax per particle (and hence per droplet) is then obtained as

$$M = C_{\text{m}} \cdot V_{\text{d}} = \rho \cdot \frac{\pi}{6} \cdot d_{\text{p}}^3. \quad (2)$$

Now Eq. (1) can be written as

$$f_{\text{ice}}(T) = 1 - \exp\left(-n_{\text{m}}(T) \cdot \rho \cdot \frac{\pi}{6} \cdot d_{\text{p}}^3\right). \quad (3)$$

It should be mentioned here that the relationship presented in Eq. (2) was also used to obtain the mass of Snomax per droplet for the particle methods (i.e., AIDA, FINCH, LACIS and PINC) shown in Fig. 1. Please note that Eqs. (2) and (3) are valid for size-selected particles, i.e., for cases where, during one experiment, particles of the same d_{p} are used, or for which, alternatively, a mass mean d_{p} can be determined.

In Hartmann et al. (2013) experiments had been conducted such, that not all of the examined droplets contained INM. It is obvious that this occurs when the number of INM present in an ensemble of droplets is smaller than the number of droplets. In general, when producing particles or droplets from a suspension, all present INM are distributed randomly over the produced particles/droplets, following Poisson distribution (for details see Hartmann et al., 2013):

$$\lambda = -\ln(1 - f_{\text{ice}}^*). \quad (4)$$

While λ represents the average number of INM per particle/droplet, f_{ice}^* denotes the fraction of particles/droplets which contain at least one of the INM. For $\lambda = 4.7$, 1% of all particles/droplets do not contain any INM ($f_{\text{ice}}^* = 0.99$). At $\lambda = 2$, f_{ice}^* is only 86%. $f_{\text{ice}}^* < 1$ shows up in the measurements when $f_{\text{ice}}(T)$ levels off in a plateau for temperatures below about -12°C , where in the plateau region $f_{\text{ice}}(T) = f_{\text{ice}}^*$. For the present study, it was possible for most instruments to run experiments such that a plateau with $f_{\text{ice}}^* < 1$ could be observed for at least one data set. This occurs when there are droplets that contain no INM, which can occur for suspensions with correspondingly low concentrations or for particles of respective sizes which might consist of biological material without containing an INM. In Hartmann et al. (2013), λ was parameterized as a function of d_{p}^3 , i.e., proportional to particle volume, and data obtained in this study will be compared to this parameterization (see Sect. 5.1).

Different methods examine different numbers of droplets. Depending on the number of droplets examined in a particular experiment, an additional uncertainty in the measurements appears for those experiments where $f_{\text{ice}}^* < 1$, based on

the fact that a comparably small number of INM is Poisson distributed to all particles/droplets. This is shown exemplarily for four different values of $f_{ice}^* < 1$ and a range of droplet numbers in Fig. 2, where the standard deviations represent theoretically predicted uncertainties which are due to the examination of only a limited number of droplets. For calculation of these values, 1 million droplets were evaluated in all cases. (To give an example, for a case when the simulation was done for 100 droplets, it was done 10 000 times, and the standard deviation was taken from the results of these 10 000 calculations.) At e.g., $\lambda = 0.5$, when 50 or 100 droplets are examined, the relative standard deviation is 17 and 12 %, respectively, while it decreases to 3 % when 2000 droplets are examined. This clearly shows that the measurement uncertainty decreases with an increase in the number of droplets examined as an ensemble. This was examined here to acquire a measure for the uncertainty that can be expected for the different data sets presented in the following.

4 Measurements and results

4.1 Determination of the Snomax density and of the size of bacterial fragments

As demonstrated in Sect. 3, the density of Snomax particles is needed for the data evaluation. The effective density of these particles (ρ_{eff}) was determined by using a combination of mobility and aerodynamic measurements. For the measurements, particles were produced using the same atomizer described above, and a DMA was used to select particles sizes of either 320 or 550 nm. Behind the DMA, the mass distribution of the Snomax particles preselected with the DMA was measured with the Aerosol Particle Mass Analyzer (APM-II KANOMAX, Model 3601). ρ_{eff} was obtained from the combined measurements of particle electrical mobility d_p and mass M :

$$\rho_{eff} = \frac{6\overline{M}}{\pi\overline{d_p}^3}, \quad (5)$$

where $\overline{d_p}$ and \overline{M} are the average mobility diameter and average mass of the singly charged Snomax particles. The measurements were done at 10 differently concentrated Snomax suspensions (from 0.1 to 5 g L⁻¹). Figure 3 shows the values of ρ_{eff} plotted as a function of concentration. Note that ρ_{eff} is an apparent density and may include the effect of porosity and particle shape (see McMurphy et al., 2002). A variation in ρ_{eff} is seen for the different examined particle sizes and also for the differently concentrated Snomax suspensions, but it is very pronounced only for concentrations which were much lower than those used in our study. The examination of only two different particle sizes is not sufficient to derive a trend for ρ_{eff} with size, and hence it was decided for this study to use the average value of 1.35 g cm⁻³ for the data evaluation.

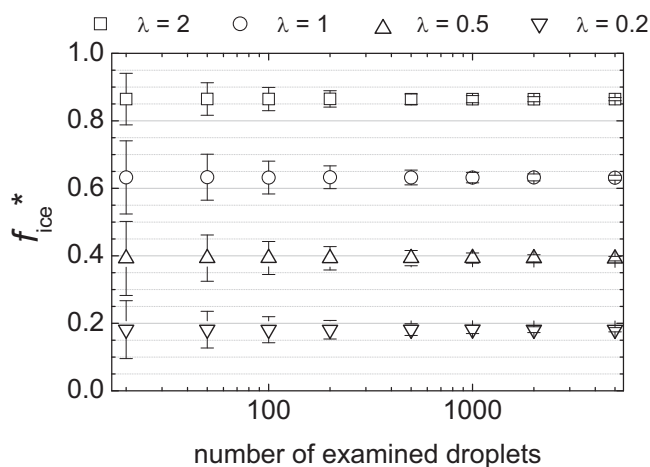


Figure 2. Average f_{ice}^* and the respective standard deviation for different numbers of examined droplets and for different values of λ , obtained by theoretical considerations.

Furthermore, as mentioned above, it was assumed that spherical particles result when sub-micron Snomax particles are produced from suspensions followed by drying. Snomax consists not only of non-viable bacteria, but also of nutrient remnants of the culture medium and of material from the interior of broken bacteria, all of which is present in a Snomax suspension. It is known that *P. syringae* bacteria themselves are rod shaped with a diameter and length roughly below 1 and 2 μm , respectively (Morris et al., 2004). Möhler et al. (2008) and Hartmann et al. (2013) both found, when using a particle generation method similar to the one used here, that a slightly elevated amount of Snomax particles was produced at sizes of roughly 800 nm (interpreted as whole bacterial cells), while a large amount of particles was produced at sizes down to below 100 nm. We will discuss in the following paragraphs that these smaller particles also contain ice nucleation active protein complexes originating from *P. syringae* bacteria, together with other substances contained in Snomax.

For the production of Snomax, the *P. syringae* bacteria are freeze-dried and irradiated to make them non-viable, and during the process the bacteria might already be damaged. Particle generation with an atomizer might damage them further, due to forces appearing in the jet region of the atomizer, where the suspension fed into the atomizer is torn into droplets. However, the protein complexes responsible for the ice nucleation activity are rather small, on the order of some nanometers for group III and some 10 nanometers for the more ice-active groups I and II (see Introduction for details). These complexes retain their ice nucleation activity as long as they are still embedded in a fragment of the cell membrane, shown e.g., by the fact that Snomax particles much smaller than the original bacteria were found to be still ice-active (Wood et al., 2002; Hartmann et al., 2013).

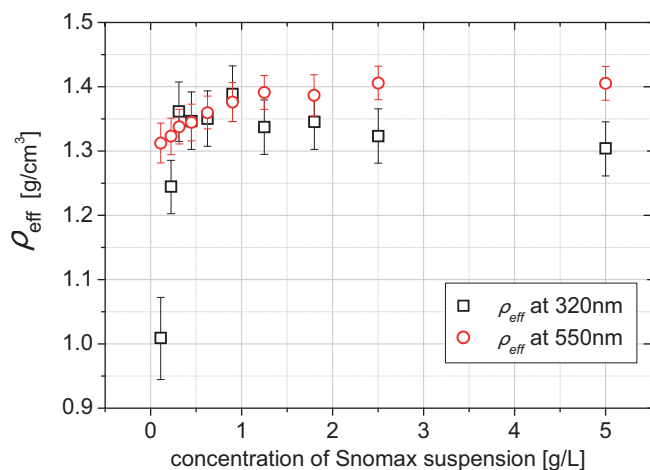


Figure 3. The effective density of Snomax measured for particles generated from differently concentrated suspensions for two different dry particle sizes.

We used a dynamic light scattering (DLS) method to determine the size of intact bacteria and of bacterial fragments present in the examined Snomax particles. For that, measurements were done with a StabiSizer (Microtrac Europe GmbH, PMX 200CS). A detailed description of the instruments and its applications can be found in Ukhatskaya et al. (2014). In short, the diameter of the fragments was determined from measurements of scattered light at an angle of 180°. The light source was a laser with a wavelength of 750 nm.

At first, the size distribution of bacteria and fragments in a Snomax suspension was examined using the DLS method directly after suspending Snomax in water. The Snomax concentration was the same used to generate dry particles in an atomizer with subsequent drying for the AIDA, FINCH, LACIS, and PINC experiments, i.e., 5 g L⁻¹. Additionally, particles were produced from these suspensions using two different particle generators, either a nozzle spray disperser or the atomizer used for this study. Dispersion of the suspensions was followed in both cases by diffusion drying, and the resulting particles were fed into a ventilated stainless steel vessel chamber (volume ~ 4 m³, temperature ~ 20 °C, pressure ~ 1000 mbar). Particles were then collected on a filter (47 mm Nuclepore® substrates, Whatman filter 111 106, 0.2 µm pore size) and subsequently washed off to produce suspensions for further examination with the DLS method.

In the following paragraph, the term “particulates” is used to denote particulate matter present in the examined suspensions, e.g., bacterial cells or fragments thereof. Results from the DLS measurements are presented in Fig. 4. The diameter (d_{DLS}) of the particulate matter present in a freshly made Snomax suspension ranged predominantly between 600 and 2000 nm. The distribution maximum is at 1000 nm. When suspensions had been sprayed with the nozzle spray dis-

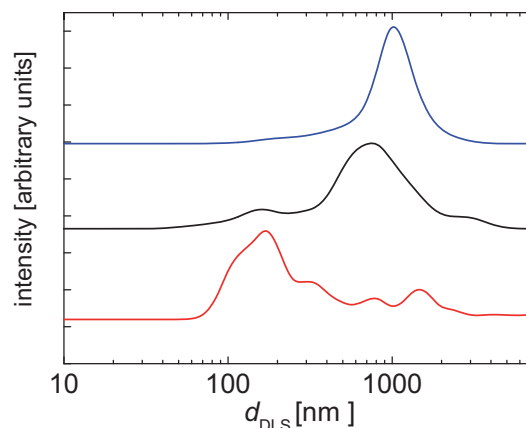


Figure 4. Size distributions of the particulate matter present in Snomax suspensions as measured with DLS. The blue curve represents the size distribution seen in a freshly produced Snomax suspension, the black and red curve show size distributions as present in particles after dispersion with a nozzle spray disperser or an atomizer, respectively.

perser, DLS detected a larger amount of particulates in the range > 400 nm, some small particulates between 50 and 400 nm and a lower amount of particulates with larger sizes. The maximum shifted slightly to 700 nm. The suspended particulate matter consists presumably of whole bacterial cells and maybe some larger fragments or crumpled cells. When the atomizer had been used, the majority of fragments appeared in the diameter range from 50 to 250 nm (with only a few fragments of the size observed before remaining). This shows that particle generation by the atomizer (even when no impaction plate was installed) disintegrated the bacterial cells to smaller pieces. While this enables particles down to a few hundred nanometers to also carry INM, it does not change the number of INM per mass of dry Snomax, as long as the protein complexes are not destroyed. This is in line with a finding presented later in this study (Sect. 5.1); namely that the distribution of INM occurs linearly with the Snomax mass over a wide range and covering both methods examining droplets made from suspensions directly and methods examining droplets activated on dry Snomax particles.

4.2 BINARY data

Figure 5 shows f_{ice} as obtained from BINARY for 14 different Snomax concentrations in the suspensions. The concentrations ranged from 10⁻⁸ to 10 mg mL⁻¹ (see legend in Fig. 5). For each of the concentrations, four or five runs including 36 droplets each were made; i.e., a total of 144 or 180 droplets was examined. For cooling rate and size of the examined droplets see Table 1. Data were recorded with a resolution of 0.1 K in the range between -40 and 0 °C. Data are only shown in the temperature range down to -20 °C, as already pure water had been observed to freeze at lower tem-

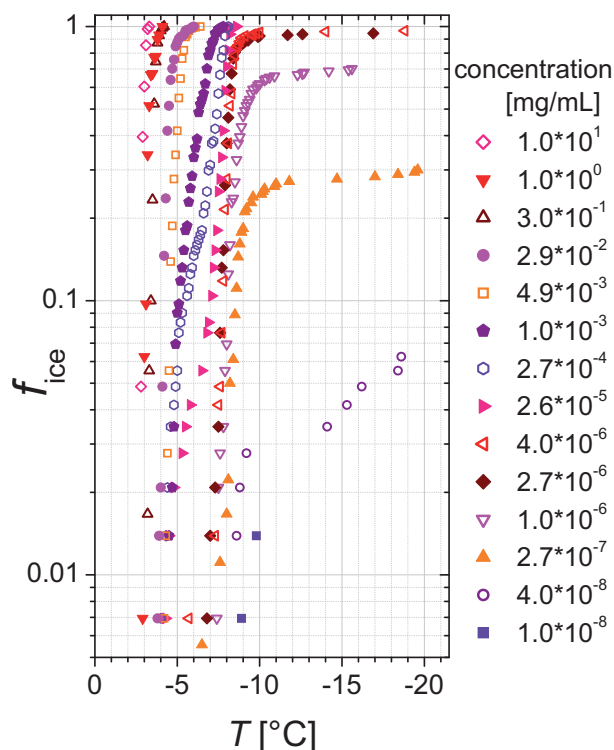


Figure 5. Frozen fractions as a function of temperature (f_{ice}) as measured by BINARY for 14 differently concentrated Snomax suspensions for droplets with diameters of $1240\ \mu\text{m}$ (i.e., $1\ \mu\text{L}$).

peratures. This could be attributed to ice nucleation induced by components in the water or by the contact of the droplets to the walls of the BINARY. It should be mentioned here that this is irrelevant for the present study as the INM in Snomax are ice-active well above $-12\ ^\circ\text{C}$.

For the highly concentrated droplets, a sharp increase in f_{ice} is seen at temperatures as high as $-3\ ^\circ\text{C}$, and after the sharp increase all droplets are frozen. The temperature at which the increase occurs decreases with Snomax concentration. For concentrations above $4 \times 10^{-6}\ \text{mg mL}^{-1}$, the maximum value obtained for f_{ice} reaches 1 at temperatures above $-10\ ^\circ\text{C}$. For lower concentrations, a plateau for $f_{ice} < 1$ is observed in the temperature range below roughly $-12\ ^\circ\text{C}$; i.e., for these concentrations not all droplets freeze. This is similar to the plateau observed in Hartmann et al. (2013) (see Sect. 3). It shows that in this concentration range only a comparably small number of INM is distributed to the generated droplets, following a Poisson distribution, such that some droplets contain no INM at all. The plateau value f_{ice}^* lowers with lowering concentration, as the number of droplets containing no INM increases. For the two lowest concentrations, the number of INM containing droplets was so low that only a few single droplets froze, making these two data sets very scarce.

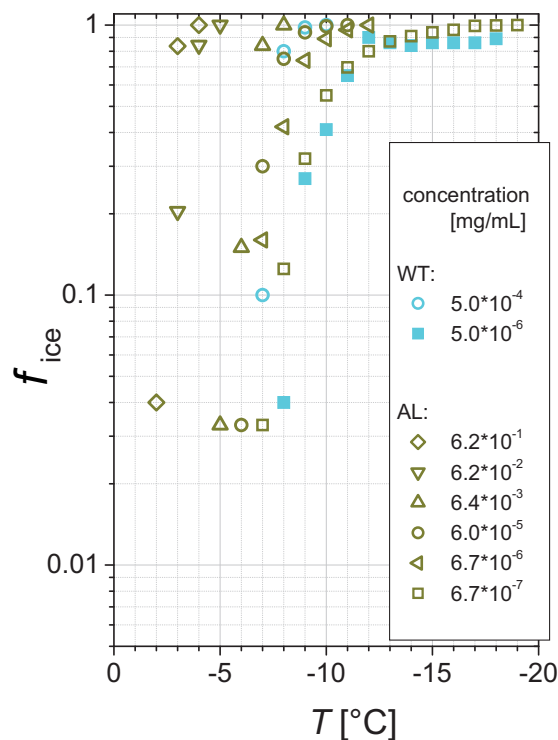


Figure 6. Frozen fractions as a function of temperature measured with AL and WT for differently concentrated Snomax suspensions. Data for the one data set which showed a plateau value below 1 are displayed with closed symbols. When the same symbols were used, the mass of Snomax per droplet was similar.

4.3 Acoustic levitator and Mainz vertical wind tunnel

Figure 6 shows f_{ice} as measured with AL and WT for different Snomax concentrations in the droplets (see legend). For ice nucleation times, sizes and numbers of examined droplets see Table 1. Data were recorded with a resolution of 1 K. Measurements are presented for six and two different Snomax concentrations for the AL and the WT, respectively. For the three highest concentrations used for experiments with the AL and the highest one used for the WT, less than five data points exist. This is due to the steepness of the increase in f_{ice} and the comparably coarse temperature resolution.

Comparable to what was found for BINARY, some of the most concentrated droplets initiated freezing at high temperatures, even already at $-2\ ^\circ\text{C}$. Again, a decrease in Snomax concentration per droplet corresponds to a shift of the freezing temperatures towards lower values. For the lowest concentration used in the WT, a plateau develops at $f_{ice}^* < 1$ in the temperature range between -12 and $-20\ ^\circ\text{C}$. In all other cases f_{ice}^* reaches 1; i.e., all droplets froze at the lowest examined temperatures. In general, the curves are somewhat more shallow than they are for BINARY. For the latter, curves which go up to $f_{ice}^* = 1$ reach that value at a temperature of $-9\ ^\circ\text{C}$ or above. This is different particularly for

the AL. Data for the lowest, second lowest, and third lowest concentration go up to $f_{ice}^* = 1$, but reach this final value only at -18 , -12 , and -11 °C, respectively. A direct comparison can be done using the data set obtained for the second lowest concentration with the AL, which is similar in mass per droplet to BINARY data with a concentration of 2.6×10^{-5} mg mL $^{-1}$. Data from the WT are similar to those from the AL. For measurements with the WT, a similar mass of Snomax in the droplets was used as in the AL (indicated by the use of the same symbols in Fig. 6). The strongest difference between AL and WT is seen for the data sets with the lowest concentration, where data for the AL increases up to 1, while a plateau is observed at 0.87 for the WT.

4.4 LACIS, FINCH and PINC

Values of f_{ice} as measured by LACIS, FINCH and PINC are shown in Fig. 7. Experimental details are again summarized in Table 1. The three different instruments all used dry particles produced from a Snomax suspension. PINC data labeled with #1 in Fig. 7 were obtained during a stay of the instrument at TROPOS, where PINC measured in parallel with LACIS. During those measurements in Leipzig, a cyclone had been installed in the particle generation setup to avoid multiply charged, i.e., larger particles. PINC data labeled #2 and #3 were measured at the ETH in Zürich, Switzerland, where particles were generated by a different atomizer than otherwise used in this study, and in one case also by a different batch of Snomax. Open symbols in Fig. 7 given for LACIS represent the data published in Hartmann et al. (2013), for which particles had also been generated using a different atomizer and a different batch of Snomax. LACIS and PINC data are given for particle diameters of 500 nm, and for LACIS additionally data for 650 and 800 nm are shown. FINCH data were measured at its home laboratory, the Goethe University in Frankfurt, Germany, for a particle diameter of 900 nm. A pre-impactor was installed at the DMA to avoid multiply charged particles.

For LACIS, error bars given in Fig. 7 correspond to standard deviations obtained from separate measurements, while for FINCH and PINC they represent standard deviations obtained from averaging several subsequently measured data points in one run. The errors were found to compare well to the uncertainties shown in Fig. 2, which had been obtained theoretically.

As for BINARY, the AL and the WT, also here a steep increase in f_{ice} is seen, however only for temperatures roughly above -7 °C. All curves show a plateau with $f_{ice}^* < 1$. This is all indicative of the fact that the mass of Snomax included in the examined particles is much lower than that included in most of the droplets examined with BINARY, the AL and the WT, resulting in a lower λ . But in the LACIS data set it can be seen already that f_{ice}^* (and λ) increase with increasing particle size.

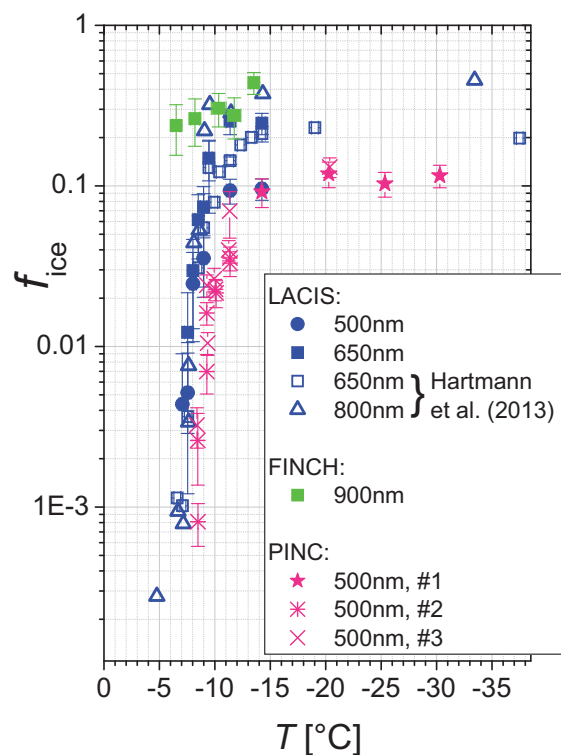


Figure 7. Frozen fractions as a function of temperature measured with FINCH, LACIS and PINC for different dry particle sizes. Open symbols given for LACIS represent the data published in Hartmann et al. (2013). PINC data labeled with #1 were taken during a campaign at LACIS, #2 and #3 denote data taken at ETH using the INUIT snomax sample and a different Snomax sample, respectively. For more details on the different data sets see Sect. A7.

A comparison of LACIS data obtained in the framework of this study with older data obtained by Hartmann et al. (2013) reveals some deviations (compare the data for 650 nm from the old and new data set), but these are still within measurement uncertainty. The new data set was obtained roughly 2 years after the old one, and the two measurements differed in the Snomax sample that was used, in the concentration of the Snomax suspension used to generate the particles and in the atomizer itself (Hartmann et al., 2013, used an atomizer following the TSI design without modifications). Similarly, a comparison can be done for PINC data obtained at two different locations (TROPOS and ETH), which also means that different atomizers and different concentrations in the Snomax suspension were used, together with two different batches of Snomax (both done at ETH). In general, the increase in f_{ice} observed by PINC occurs roughly 2 K below where it was observed for LACIS. But the PINC data obtained for the different Snomax batches and different atomizers agree well with each other. These results obtained from LACIS and PINC can be interpreted such that likely neither the atomizer used to generate the particles, nor the concentration in the suspension nor the Snomax batch had a clearly

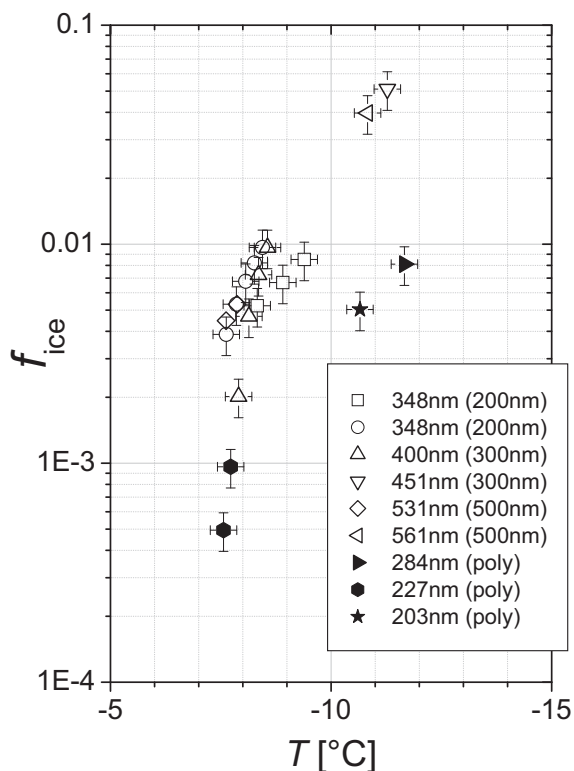


Figure 8. Frozen fractions as a function of temperature, measured with AIDA during nine different experiments. Different dry particle sizes or size distributions had been fed into the chamber. The diameter given in the legend indicates the effective volume mean diameter and, in parenthesis, the mobility diameter selected at the DMA is given in addition.

noticeable influence on the results of the measurements. It should, however, be pointed out that some participants of this study reported that Snomax was observed to show a decline in ice nucleation ability, particularly when it was stored above 0 °C for some length of time (weeks), and less so but still noticeable when it was stored frozen for several months (data not shown in this study).

f_{ice}^* for 500 nm particles examined with LACIS and PINC agree well with each other for temperatures below about -12 °C, while it was already mentioned above that PINC observed the onset of ice nucleation at lower temperatures (by roughly 2 K), compared to LACIS. This might originate in the measurement principle of PINC (see Appendix A7), where supersaturation with respect to ice and water is generated by a temperature gradient between two iced walls. For measurements at high temperatures (roughly -10 °C and warmer), it is not possible to generate high supersaturation with respect to water any more, and residence times for supersaturated conditions become very short. Hence PINC measurements in the temperature region above -10 °C might be biased by instrumental limitations.

FINCH data were taken for a particle diameter of 900 nm, and a plateau is observed close to that observed for 800 nm particles with LACIS. Droplets examined in FINCH contain roughly the same Snomax mass as droplets with the lowest concentrations examined in the AL and the WT or droplets with Snomax concentrations between 2.7×10^{-7} and 1.0×10^{-6} mg mL $^{-1}$ examined in BINARY. The respective data sets from AL, BINARY, LACIS, PINC and WT show a steep increase in f_{ice} only below -7 °C, while f_{ice} measured by FINCH is 0.2 already at -6.5 °C. Unfortunately, no FINCH data are available in the temperature range above -6 °C for further comparisons.

4.5 AIDA

Figure 8 shows data obtained with AIDA. Nine separate runs were evaluated. For each run, the particle size spectrum present in AIDA was different. While for some runs a poly-disperse particle size distribution was used, size-segregated particles were fed in for others (see legend). In all cases the complete particle size distribution from 10 to 17 000 nm was measured and taken into account to calculate total particle number concentrations and related parameters. A summary of cooling rates, particle sizes, and numbers of examined droplets is again given in Table 1.

For five of the runs presented here, expansions in the AIDA chamber were started when the temperature in AIDA was above -7 °C. For these cases, droplets were activated on the particles before AIDA was cooled to the expected onset temperature for the immersion freezing of the Snomax particles, and immersion freezing could set in as soon as the expansion cooled the chamber sufficiently. For any of these runs, a series of data points (2 up to 5), all averaged over 10 s, is presented in Fig. 8. The calculation of f_{ice} was limited to the early ice formation and growth period with ice crystals well below the size limit of about $50 \mu\text{m}$ in diameter at which settling losses may affect the measured ice crystal number concentration. For four AIDA runs, the expansions were started at a temperature of about -9 °C, so that supersaturation with respect to water, and hence droplet activation, was only reached below -9 °C. In these cases, droplets were activated at temperatures where the Snomax particles, as soon as they were suspended in the growing droplets, induced freezing at very high rates. Therefore, the formation of droplets was followed by a steep increase in the number of ice crystals, and for these runs, only the maximum value of f_{ice} is depicted in Fig. 8.

Not many data points exist in the temperature range in which the plateau would be expected; i.e., there are no data below -12 °C and four data points between -10 and -12 °C. These four points were obtained for differently sized particles and show a range of values for f_{ice} . These differences are mainly caused by a different Snomax mass contained in the droplets, i.e., by a different aerosol particle size present during the different runs. This will be addressed later.

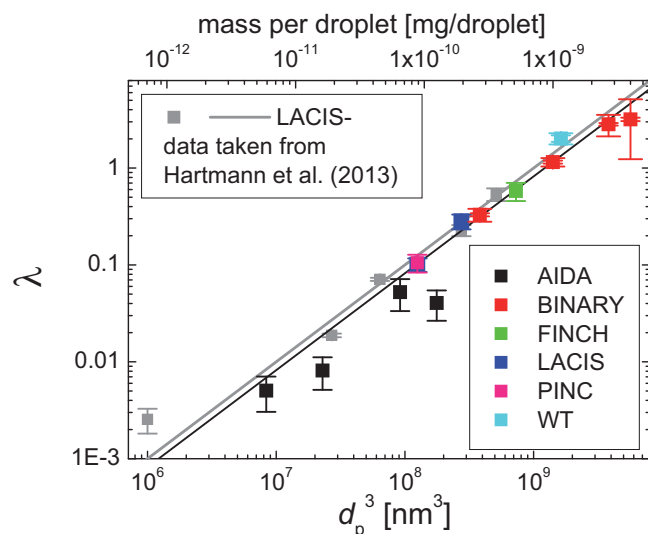


Figure 9. Average number of INM per particle or droplet as a function of the third power of particle diameter or mass per droplet, respectively, for data sets that showed a clear plateau with $f_{ice}^* < 1$. Grey symbols represent data published in Hartmann et al. (2013). The grey line is the corresponding fit function derived in Hartmann et al. (2013), which also describes the data collected in the present study well. The black line represents a fit obtained for this study (for details see text).

A steep increase of f_{ice} in the temperature range between roughly -7 and -10 °C is visible, similar to what was observed for most other instruments.

5 Comparisons

5.1 Comparing frozen fractions in the plateau region

Immersion freezing induced by *P. syringae* is known to set in well above -12 °C (mostly even above -10 °C, e.g., Yankofsky et al., 1981), and as shown for the separate instruments in Sect. 4, this was observed in the current work as well. As discussed above, some measurements were made for droplet ensembles for which not each droplet contained an INM. In these cases, a plateau formed, and the respective frozen fractions are denoted as f_{ice}^* herein. These cases are examined in more detail now. This is done following an approach introduced in Hartmann et al. (2013). For that, we used Eq. (4) to calculate λ , based on f_{ice}^* . For each instrument where the respective data were available, and there for each particle size or Snomax concentration in the droplets, an average f_{ice}^* was obtained for temperatures ≤ -12 °C. For BINARY, again only data ≥ -20 °C were considered. AIDA data were only taken at temperatures above -12 °C, and the four data points sampled between -10.5 and -12 °C were also included.

Figure 9 shows the respective data, where λ is plotted versus d_p^3 . For data from BINARY and the WT, Eq. (2) was used

to convert the mass of Snomax contained in the droplets to d_p^3 , using $\rho = 1.35$ g cm $^{-3}$. The grey symbols in Fig. 9 represent data from Hartmann et al. (2013), and the grey line is the relation given therein between λ and d_p^3 ; namely, $\lambda = F \cdot d_p^3$ (with $F = 9.995 \times 10^{-10}$ nm $^{-3}$).

The uncertainties shown in Fig. 9 are taken from the measurement uncertainties of f_{ice} . These uncertainties are similar to those which can be obtained based on the number of droplets counted by the different instruments, besides for the two suspension methods AL and BINARY. For these two, uncertainties which are based on counting statistics are larger than the experimental uncertainties of the measurements, likely due to the comparably low number of examined droplets. Hence, for these two, also uncertainties taken from the analysis presented in Fig. 2 are shown in Fig. 9, displayed with broader error bars.

It can be seen that the data point for the largest λ from the BINARY data set deviates from the linear relationship seen for most data points in Fig. 9. At large λ values, small deviations in f_{ice} cause a large uncertainty in λ , due to the strong non-linearity of λ as function of f_{ice} , particularly for $f_{ice} > 0.95$, i.e., for $\lambda > 3$. Hence the data point from BINARY for the largest λ is less well constrained than the others, and data for $\lambda > 3$ can not be expected to follow a linear behavior as otherwise displayed in Fig. 9. AIDA data included in Fig. 9 deviate towards lower values. However, because of the fast ice crystal growth at temperatures around -10 °C already mentioned above, in a single AIDA expansion run it was not possible to measure the full transition of f_{ice} from its steep increase below about -10 °C to the plateau value. Only four data points were obtained at temperatures between -10.5 and -12 °C, where the plateau was not yet fully reached according to most other data sets. This could explain the slight low bias in λ seen for AIDA data.

Two new fits for data shown in Fig. 9 were also done for data points obtained in this study for $T < -12$ °C and $\lambda < 3$. For that, data obtained in this study was used together with data from Hartmann et al. (2013) in one case, while for the other case data from Hartmann et al. (2013) was excluded. For these two cases, values of F of 8.21×10^{-10} nm $^{-3}$ and 8.18×10^{-10} nm $^{-3}$ were obtained, respectively. This is less than 20 % lower than the respective value derived based on data from Hartmann et al. (2013) alone. The resulting fits are very similar and are depicted together as one black line in Fig. 9. Generally, it can be said that data obtained in this study align well with those from Hartmann et al. (2013).

In general, the data presented in Fig. 9 confirm that the distribution of INM over the droplet population can be well described using a Poisson distribution. When a sufficiently small number of INM is distributed over a sufficiently large number of droplets, so that not all of the generated droplets contain an INM, a plateau at $f_{ice}^* < 1$ occurs below -12 °C. Moreover, the presented analysis included the determination of d_p^3 for BINARY and the WT based on the mass and density

of Snomax in the droplets. The fact that a good comparison was found with data from FINCH, LACIS and PINC justifies the value used for the density of Snomax, where, however, it should be pointed out that values for ρ_{eff} between 1.2 and 1.5 g cm⁻³ would only lead to a deviation in the Snomax mass per droplet of 10 % for the suspension methods, which would result in error bars still being located within the respective symbols depicted in Fig. 9.

5.2 Comparing active site densities per mass, n_m

5.2.1 BINARY

Here we first show and discuss values of n_m (i.e., INM per unit of dry Snomax mass) as derived from BINARY data, and then compare and discuss the respective values derived from measurements of all other instruments.

Figure 10 shows n_m derived from measured f_{ice} using Eq. (1). Although 9 orders of magnitude were spanned with respect to the Snomax concentrations in the examined suspensions, data on n_m for all these different concentrations fall nicely together. After a first increase in f_{ice} starting at roughly -2°C , a slight shoulder is visible in the data at $n_m \sim 10^6 \text{ mg}^{-1}$ and $\sim -6^\circ\text{C}$. A second strong rise in n_m is seen in the temperature range from -7 to -9°C , leveling off at a value of $n_m \sim 10^9 \text{ mg}^{-1}$.

The two clearly distinct rises show that the ice activity comes from two clearly different types of INP (i.e., from two distinct types of INM or more specific two different protein complexes (remember that we are dealing with *P. syringae*)). In each of the two temperature ranges, one type is ice-active, corresponding to different groups or classes as described above (see Introduction). Group III behavior is seen clearly in the temperature range below -7°C . All INM active above -7°C will be ranked as group I, as no further clear discrimination between different types of INM can be seen in this temperature range. In both temperature ranges, below and above -7°C , a rise of f_{ice} as well as of n_m is distributed over a certain temperature range, as even within one group of INM there are small differences between the different protein complexes. As the temperature lowers, more and more of the respective INM induce ice formation. When a plateau is reached, all INM of one group which are capable of inducing ice have done so. Therefore the plateau reveals how many INM per mass of dry Snomax are present in the sample. As mentioned above, this is $\sim 10^6 \text{ mg}^{-1}$ and $\sim 10^9 \text{ mg}^{-1}$ for the two groups of INM observed here.

For $T > -6^\circ\text{C}$, only droplets made from suspensions with concentrations $> 10^{-5} \text{ mg mL}^{-1}$ froze. This is in line with the fact that the more ice-active group I-INM occur roughly 3 orders of magnitude less frequent than the less ice-active ones. For a concentration of $10^{-8} \text{ mg mL}^{-1}$, even the more abundant group III-INM were hardly present in any of the droplets (see Fig. 5), and hence at concentrations $< 10^{-5} \text{ mg mL}^{-1}$, it can be expected that the more ice ac-

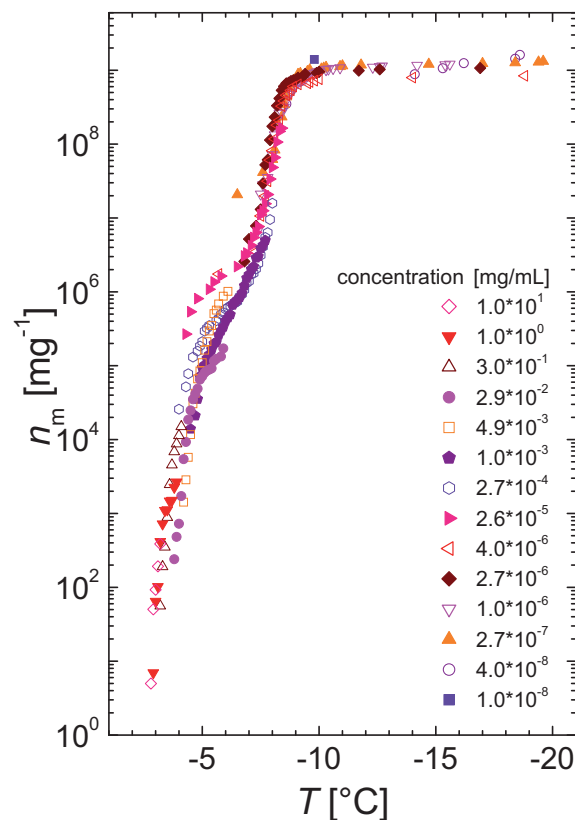


Figure 10. BINARY data represented as number of INM per dry Snomax mass, n_m , as a function of temperature, for all data shown in Fig. 5 and using identical symbols.

tive but less abundant group I-INM ceased to populate the droplets.

5.2.2 Overall comparison

In Figure 11, values for n_m are shown for all f_{ice} data presented in Sect. 4, where Eqs. (1) or (3) were used to obtain n_m for those methods which examined droplets from suspensions or size-segregated particles, respectively. The panel on the left of Fig. 11 gives an overview of all data, while the panel on the right is an enlargement of a part of the former.

Data of all different instruments are close to each other, with some exceptions. As described above, also here a region can be seen in which f_{ice} increases linearly for most data sets, in the temperature range from roughly -7 to -9°C , and the plateau in n_m is visible roughly below -12°C . Of all data down to -12°C , and for n_m between $2 \times 10^6 \text{ mg}^{-1}$ and $7 \times 10^8 \text{ mg}^{-1}$, 72 % of all data points fall within a 1 K band and 78 % within 2 K band around the mean. In the region where n_m forms a plateau, all data are found in the range from $7 \times 10^8 \text{ mg}^{-1}$ to $2.1 \times 10^9 \text{ mg}^{-1}$, i.e., less than a factor of 3 apart, with an average value of $1.4 \times 10^9 \text{ mg}^{-1}$. Hence, apart from issues which will be discussed below, data from the instruments included in this study agree quite well.

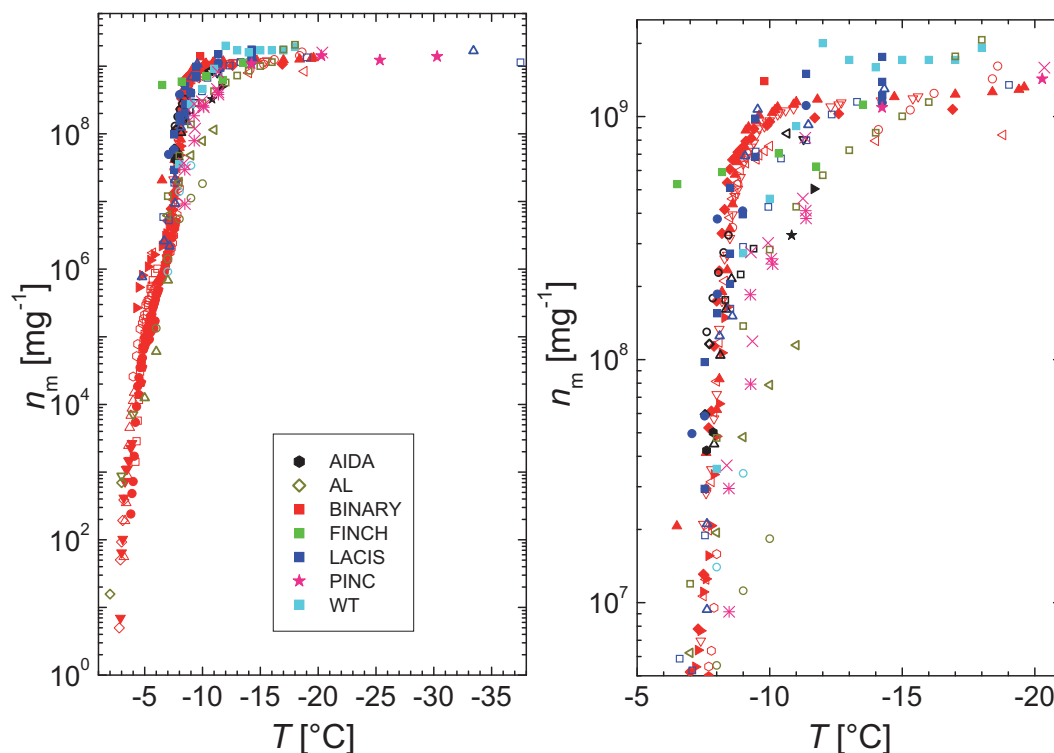


Figure 11. Number of INM per dry Snomax mass as a function of temperature, derived from measured f_{ice} of all instruments, i.e., for all data shown in Figs. 5 to 8. BINARY data are solely displayed in red, but otherwise the same symbols and color codes are used as in Figs. 5 to 8; i.e., in all cases data from one instrument are always displayed in a single color. The right panel is similar to the left, zooming in on values for $5 \times 10^6 \text{ mg}^{-1} < n_m < 2.5 \times 10^9 \text{ mg}^{-1}$ and on temperatures $> -21^\circ\text{C}$.

For the AL, all values for n_m below -8°C are clearly lower than those from all other instruments. A similar effect is also seen, albeit only weakly, for data from the high concentrated droplets examined in the WT, which, however, might be traced back to the temperature resolution of only 1 K of that data set. The observed lower n_m values for the AL are related to the fact that the respective curves for f_{ice} did increase less steeply than those reported by other instruments and only leveled off below -10°C (Sect. 4.3 and Fig. 6). Data from the WT obtained for the low Snomax concentration increase almost as steep as the bulk of the data in the temperature range below -10°C and form a plateau in n_m with values slightly above the bulk of the data. Here, the comparatively low number of examined droplets corresponds to a comparably large uncertainty in the data which causes these data to agree with the bulk within measurement uncertainty (see Sect. 3 together with Figs. 2 and 9).

FINCH, as already discussed for f_{ice} , did not detect the steep increase in n_m between -7 and -9°C . Instead, n_m measured at -6.5°C does not differ significantly from those values measured between -8 and -12°C , while n_m measured at -13°C is almost twice as large as values measured at higher temperatures.

As discussed above, a somewhat delayed increase for the PINC data compared to the bulk is visible. This might originate in the fact that the instrumental limitations impede immersion freezing measurements at temperatures above -10°C and cause very short residence times at these comparatively high temperatures. It should also be mentioned that all of the PINC data for $T > -12^\circ\text{C}$ were done with a different atomizer; however, this is likely not the reason for the deviation, as data for $T < -12^\circ\text{C}$ are in agreement, no matter which atomizer was used. PINC data in the plateau region agree well with the bulk. It should be mentioned that n_m values for $T < -12^\circ\text{C}$, i.e., in the plateau region, when derived from PINC and also from LACIS data, show a scatter of roughly a factor of up to 1.5 when these measurements were done repeatedly at the same temperature. The observed scatter is larger in the temperature range above -9°C , particularly for LACIS data, which, however, originates from the steep increase in f_{ice} and n_m at these temperatures.

Above -10°C , n_m derived from AIDA measurements agree with the bulk of the data. In the range below -10°C , the two data points obtained from measurements examining polydisperse particles are among the lowest ones found at the respective temperatures, and they are lower than the two AIDA data points from monodisperse measurements done in

this temperature range by about roughly a factor of 2. A possible explanation could be that polydisperse measurements in AIDA include very small aerosol particles for which the distribution of INM might not follow a Poisson distribution.

When the above explicitly mentioned data are excluded from the examination, a much larger fraction of all data is included in the 1 and 2 K bands described above. A discussion motivating the exclusion of these data is given in the section following below. These data are BINARY data for $T < -20^{\circ}\text{C}$, which generally had been excluded in the analysis presented herein, data from the AL for $T \leq -9^{\circ}\text{C}$, the two polydisperse measurements done with AIDA at $T < -10^{\circ}\text{C}$, the FINCH data point at -6.5°C and PINC data for $T > -10^{\circ}\text{C}$. When these data are excluded, of all data down to -12°C and for n_m between $2 \times 10^6 \text{ mg}^{-1}$ and $7 \times 10^8 \text{ mg}^{-1}$, 86 % of all separate data points fall within a 1 K band and 91 % within a 2 K band around the mean, while, as before, all data in the plateau region are less than a factor of 3 apart from each other.

6 Discussion

The comparison introduced in the study presented here taught us some lessons. But before we discuss them, we want to mention that, unless otherwise stated, the following remarks are generally valid also for other suspension methods or other particle methods, not only for those included in this study.

Based on the results from the current work, we propose that Snomax is an appropriate material to be used as a test substance for future studies, at least when carefully shared and prepared. The majority of the data obtained for this study was collected using Snomax from the same batch and using the same atomizer. However, data measured by LACIS and PINC using different Snomax batches, atomizers and suspension concentrations have also been included here. Given that none of the variations in sample generation and preparation noticeably influenced the measurement results, we suggest that Snomax could be used as a standard reference aerosol for future comparisons. This can also encourage others to compare respective results with those published herein.

We also note that the examination of the complete temperature range can yield additional information, compared to the examination of only the temperature range in which a strong increase in f_{ice} is observed. The range in which the strong increase is observed is important when temperature accuracy is examined. However, also temperature ranges were observed in which no additional ice nucleation was observed, i.e., in which n_m was rather constant (around -6°C and below -12°C). When f_{ice} measured in these temperature ranges is below 1, then these measurements, made for Snomax or other substances, can give information about the counting accuracy of the instrument or about instrumental issues. To obtain the respective measurements with values of

f_{ice} below 1, either sufficiently low concentrated suspensions for suspension methods, or a respectively small particle size for the particle methods has to be chosen, where, however, in our study all particle sizes which could possibly be chosen with a DMA were sufficiently small.

In our study, measurements in the plateau region below -20°C revealed a clear increase in f_{ice} for the BINARY data sets obtained for the four lowest concentrations. This increase occurred well above the homogeneous nucleation temperature of -38°C , where an increase is unavoidable. These BINARY data were neither displayed here, nor were they included in the analysis of the ice nucleation behavior of Snomax. The observed increase was either caused by impurities in the water used for dilution or by the substrate surface itself, as evidenced by the fact that the respective n_m values did scale with the dilution factor, i.e., a reduction of Snomax concentration by a factor of 10 resulted in an increase in the observed n_m values by a factor of about 10. A possible influence of the substrate is avoided in AL and WT. But generally, for suspension methods the possibility of an influence of impurities in the water increases with the size of the examined droplets. Another disadvantage of the suspension methods is, that usually only a smaller number of droplets can be examined, compared to the particle methods. This number of droplets still differs between different suspension methods; e.g., while BINARY measurements are automated and examine 36 droplets in one run, in both AL and WT single droplets are examined separately consecutively.

In Figure 11, it can be seen that data for the more ice-active group I-INM were only reported by the AL and BINARY, indicating an advantage of the suspension methods. At the same time, a weakness of the particle methods is apparent, which is due to reaching the lower limits of detection. Suspension methods can vary the amount of ice nucleating material over a wide range. Samples exist, in which only a very small fraction of all particles carries an INM (or, alternatively, an ice-active site on mineral dust particles), as is the case for group I-INM in Snomax, for example. In contrast, when particles are generated for the particle methods, they are restricted in their upper size (and mass) by the particle generation method. Additionally, particles in the supermicron size range are lost, due to impaction and/or sedimentation, in the particle generation and instrument set-up, increasingly so with size. In order to generate a particle population in which 50 % of the particles carry at least one of the group I-INM observed in Snomax (i.e., have a λ of 0.5 for these), they would have to have a diameter of roughly $8 \mu\text{m}$. As mentioned above, however, particles in this size range are difficult to generate and sample. Hence particle methods are limited in their ability to detect rarely occurring INM (or ice-active sites on mineral dusts). Among these instruments, AIDA can detect the lowest ice crystal concentrations. The largest particle size examined up to date in FINCH is 900 and 1000 nm in LACIS and PINC. This may not represent the absolute upper size limit detectable in these instruments,

but instrument and detector limitations make it challenging to sample super-micron particles.

In the present study we used a time-independent approach to compare data from the different instruments. Based on our results as presented in Fig. 11, where data from the fastest (LACIS) and slowest (BINARY) instrument agreed well, it can be argued that a strong time dependence for Snomax is unlikely. This would also be expected from the steep dependence of f_{ice} with temperature.

However, this likely does not apply for all ice nucleating substances, and examination of the time dependence can be informative. AIDA and BINARY can vary their cooling rates, ranging from 1 to 3 K min⁻¹ for AIDA and from 0.1 to 10 K min⁻¹ for BINARY. The WT allows to record the time when the freezing occurred; however, up to now only cumulative results after 30 s have been used. And examining a time dependence is not possible or can be done covering only a smaller range for AL, FINCH, LACIS and PINC.

In Section 5.2.2, it was discussed that some n_m data deviated noticeably from the bulk of the data. This included BINARY data below -20°C , as discussed above in this section. Also concerned were data measured with AL at temperatures of -9°C and below, two data points measured with AIDA for polydisperse aerosols, the FINCH data point at -6.5°C and data measured with PINC for temperatures above -10°C . In the following paragraphs, we will discuss specific issues which might have been the cause for these observed deviations.

- *Acoustic levitator.* We first want to address the AL. Some of the AL data agree well with the bulk of the data, but measurements below -8°C show noticeably lower values for n_m . These measurements were done for droplets with lower concentrations of Snomax per droplet, which only freeze at temperatures below about -7°C . An explanation might be the following: in the AL, the temperature is measured directly at the surface of the droplets by an infra-red thermometer. The signal which is taken to indicate first ice nucleation is the start of an increase in the droplet temperature, resulting from the release of latent heat during ice formation. The droplets examined in the AL are rather large (2 mm in diameter), and nucleation most likely takes place in the interior of the droplets. When the first ice nucleation occurs, it will take some time until the related increase in droplet temperature propagates to the droplet surface. Meanwhile the droplet is continuously cooled down and hence the temperature at which the increase in the droplet temperature is detected is somewhat below that at which the first ice nucleation took place.

This effect might not be negligible in particular for Snomax experiments where freezing takes place in a temperature range not far below 0°C . There the cooling rate of the droplets in the AL is very fast; i.e., they cool down from 0 to -10°C within 10 s; i.e., the cooling rate is

1 K s⁻¹ (see Fig. A1). For droplets in which ice is nucleated at temperatures at and above -8°C , freezing may proceed so very fast that this effect does not play a noticeable role, but at lower temperatures it might become apparent by a less steeper slope of f_{ice} and n_m .

Another reason for the observed deviations in the AL data to others could be that the droplets, which are cooled down very fast during the first 10 s, are still warmer in their bulk than at their surface. Hence, by the time the interior reaches a temperature which is sufficiently low for ice nucleation to take place, the droplet surface is already colder.

These deviations will be examined in more detail in the future, and likely a calibration of this effect, maybe even based on the herein presented Snomax data set, seems feasible to account for the offset in temperature in the respective temperature range.

- *AIDA.* For AIDA, n_m data obtained for polydisperse measurements at $T < -10^\circ\text{C}$ were at the lower end of values observed at the respective temperatures. This was discussed in Sect. 5.2.2, and we only repeat here that the particles which were used in these experiments were the smallest ones used in this study, and possibly it might not be valid to assume that the distribution of INM to these particles still followed a Poisson distribution. This could be checked in future experiments with size-selected particles below 200 nm diameter.
- *FINCH.* FINCH was the only instrument which did not detect the steep increase in n_m between -7 and -9°C , and also detected an increase in n_m by a factor of 2 between -12 and -13°C , at a temperature where no additional new ice activity is expected from Snomax INM. All of the data presented in this study were taken during one experimental run, for which temperatures were scanned comparatively fast, which might have caused problems. However, as it was not possible to obtain additional data prior to the submission of this study, a more detailed discussion of possible issues in FINCH is not possible.
- *PINC.* At temperatures above roughly -10°C , n_m determined from PINC measurements were clearly lower than other values for n_m obtained for this study. The upper sampling temperature used in PINC for this study was -8°C . In order to achieve supersaturation at the sample position at -8°C , the warm wall needs to be at temperatures warmer than -3°C , which makes the mass transfer for ice from warm to cold wall quite high, leading to anomalous ice crystal counts from falling frost particles growing on the cold wall. This results in the limit of detection being too high to quantify ice formation at temperatures above -8°C . However, below -8°C , data contaminated by frost falling off the

walls can be distinguished and excluded. A further issue might originate in the measurement principle of PINC (see Appendix A7), where supersaturation with respect to ice and water is generated by a temperature gradient between two iced walls. For measurements at high temperatures (roughly -10°C and warmer), it is not possible to generate high enough supersaturation with respect to water any more, and residence times for supersaturated conditions become very short. Hence PINC measurements in the temperature region above -10°C might be biased by instrumental limitations.

7 Comparison of n_m averages with parameterizations from literature

In this section we compare two existing parameterizations from the literature to those obtained in the current work. In a first step, average n_m values were derived from our data. Based on the instrumental peculiarities discussed above, some data were excluded from the averaging procedure, as described in Sect. 6. The remaining data from each of the instruments were averaged separately. All values for n_m were averaged in 1 K bins below -12.5°C and in 0.5 K bins above. The resulting seven data sets were then averaged to yield overall n_m values representative for this study. The results are shown as black circles in both panels of Fig. 12. According to the averaging procedure, each instrument contributed to the average with an equal weight, and the error bars depicted for n_m reflect the deviation based on averaging the seven data sets. The uncertainty shown for the temperature represents $\pm 0.6\text{ K}$. All separate data points that were included in the averaging are shown in light grey in the background.

Two existing models are compared to the average data in Fig. 12. The red line represents the following curve:

$$\begin{aligned} n_m(T) &= \frac{6F}{\pi\rho} (1 - \exp(-t \cdot A (\exp(B \cdot T)))) \\ &= 1.4 \times 10^9 \text{ mg}^{-1} \\ &\quad \left(1 - \exp\left(-2 \times 10^{-10} \left(\exp\left(-2.34^{\circ}\text{C}^{-1} \cdot T\right)\right)\right)\right) \quad (6) \end{aligned}$$

This was obtained by equalling the fractions of unfrozen droplets as described with the CHESS-model in Hartmann et al. (2013) to those as described in Eq. (3), with T in $^{\circ}\text{C}$, $\rho = 1.35 \text{ g cm}^{-3}$ (see Sect. 5.1) and values taken from Hartmann et al. (2013): $F = 9.995 \times 10^{-10} \text{ nm}^{-3}$, $A = 9.99 \times 10^{-10} \text{ s}^{-1}$, $B = -2.34^{\circ}\text{C}^{-1}$ and $t = 0.2 \text{ s}$ (the respective nucleation time in LACIS, on which the determination of A and B was based). (The resulting n_m represents a time independent parameter, while a time-dependence had been incorporated in the CHESS-model originally.)

The blue line was obtained as follows: a model based on classical nucleation theory, the Soccer ball model (SBM) as described in Niedermeier et al. (2014), was used to calculate f_{ice} for a nucleation time of 10 s (which is roughly a mean

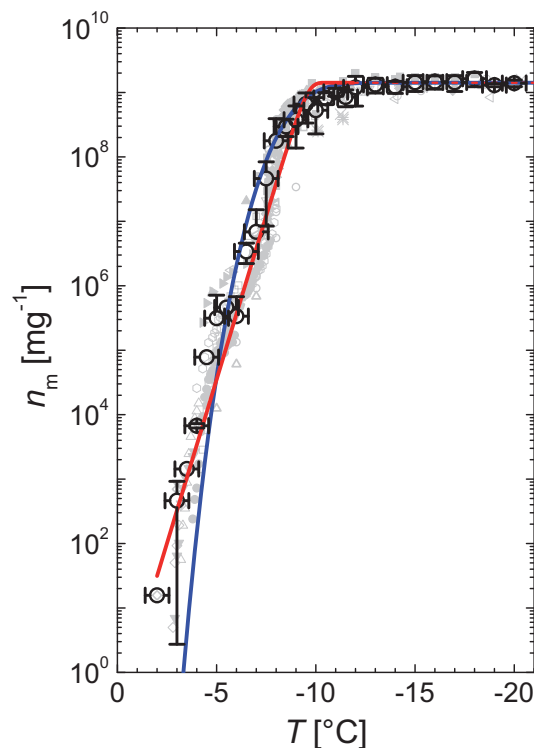


Figure 12. Average n_m values (black circles) overlying all separate data points which were included in the average (shown as background in light grey), together with fits obtained from a time-independent variant of the parameterization given in Hartmann et al. (2013) (red curve, see Eq. 6) and in Niedermeier et al. (2014) (blue curve).

value for the methods used in this study). A slight time dependence of the ice nucleation process for Snomax can be observed (as discussed in detail in Budke and Koop, 2015). But as a change of the nucleation time of a factor of 10 shifts the freezing curve by roughly only 0.3 K (and a factor of 100 by 0.6 K etc.), we use the mean nucleation time given above as being representative for the whole study and otherwise neglect a time dependence. The contact angle distribution used for Snomax was $\mu_0 = 0.595 \text{ rad}$ (34.1°) and $\sigma = 0.04 \text{ rad}$ (2.3°) for the mean contact angle and the standard deviation (Niedermeier et al., 2014). f_{ice} as calculated by the SBM was then converted to n_m using Eq. (3). n_m was derived for particles of sizes with 500, 1000, 1500 and 2000 nm (i.e., for different λ values), and as to be expected, the resulting n_m showed to be independent of the particle size. The result of these calculations is seen as a blue line in Fig. 12.

The maximum average value of n_m of $1.4 \times 10^9 \text{ mg}^{-1}$ coincides very well by both approaches presented in Fig. 12. But both parameterizations were originally made to describe the immersion freezing behavior of the more abundant but less ice-active INM, so that the shoulder in n_m at roughly -6°C is not represented explicitly. A further deviation occurs in the region where the steep increase in n_m levels off

into the plateau (roughly around -10°C), where the bend in the curve based on Eq. (6) (Hartmann et al., 2013) is slightly sharper than that seen in the average values. Another small deviation can be seen for the three lowest average n_m values below $2 \times 10^3 \text{ mg}^{-1}$, which are underestimated by the SBM. However, with the exception of these three values, both parameterizations describe the average data well over the whole course within a temperature uncertainty of $\pm 0.6 \text{ K}$ (95 % confidence range) in the entire range in which an increase of n_m is seen. When judging the deviation in relation to n_m , it is less than a factor of 2 at all temperatures at which measurements were made, again besides for the SBM parameterization above -5°C . But the INM which are ice-active at these high temperatures, i.e., belonging to group I, can be expected to be of a minor if not negligible atmospheric relevance, due to their scarce occurrence which was already noted e.g., by Yankofsky et al. (1981). Therefore, a new parameterization taking this second type of INM explicitly into account was omitted in this study. Instead it can be concluded that most of the data measured in the framework of this present study are in agreement with already existing parameterizations, where the two parameterizations described here represent a time-independent one (Eq. 6) and one in which a time dependence of the freezing process technically is accounted for (SBM).

8 Summary and conclusions

In this study, data obtained for immersion freezing from seven different measurement methods and instruments were compared to each other. These instruments included methods examining droplets which were made from suspensions directly (suspension methods), which were an acoustic levitator (AL), an optical freezing array (BINARY) and a wind tunnel (WT). The remaining four instruments all examined INP (particle methods) and included an expansion chamber (AIDA), a flow tube (LACIS) and two ice nucleation counters (FINCH and PINC). The comparison was done within the research unit INUIT (Ice Nucleation research UnIT), and focused on the examination of ice nucleation up to comparably high temperatures, where the highest temperatures probed with the different instruments were in the range from -2 to -8°C . Due to its ability to induce ice nucleation at these high temperatures, Snomax was used as the test substance. This is a commercially available product containing ice nucleation active protein complexes originating from *P. syringae* bacteria. Care was taken to use similar droplet and particle generation techniques and Snomax from the same batch as far as possible.

To enable a comparison, all data were represented as number of ice-active entities per mass of examined (dry) substance (n_m), an approach taken from Vali (1971). In general, the observed curve for n_m is in agreement with the vast body of literature existing for *P. syringae* and Snomax, for which it is known that ice nucleation active protein com-

plexes (i.e., ice nucleation active macromolecules, INM) induce the freezing, and that more and less ice-active types of INM exist, i.e., group I and group III protein complexes. A sharp increase in measured frozen fractions and n_m was seen starting at temperatures below -2°C , leveling off in a shoulder at -6°C , followed by a second steep increase from -7 to -9°C . The two increases show the temperature ranges in which two differently sized (and differently ice-active) INM types become ice-active. A plateau in n_m developing below -12°C yielded that the number of group III-INM in the examined Snomax sample was $1.4 \times 10^9 \text{ mg}^{-1}$. The more ice-active group I-INM were 3 orders of magnitude less abundant, i.e., occurring in numbers of $\sim 1 \times 10^6 \text{ mg}^{-1}$.

Data determined for this study mostly were found within a range of 1 K for temperatures above -12°C (86 % after exclusion of some outliers). For temperatures below -12°C , they were found in a range from $7 \times 10^8 \text{ mg}^{-1}$ to $2.1 \times 10^9 \text{ mg}^{-1}$, i.e. less than a factor of 3 apart around the average value of $1.4 \times 10^9 \text{ mg}^{-1}$. Pronounced differences were only seen for some instruments in some temperature ranges, including the AL below -9°C , BINARY below -20°C , FINCH above -8°C , PINC above -10°C and two AIDA expansions made for polydisperse particles below -10°C . Possible reasons for the observed deviations are discussed in the text, together with general advantages and disadvantages of suspension and particle methods.

In the present study, besides the above discussed deviations, data agreed well over the whole temperature range in which measurements were made. In the temperature range below -12°C , where data from five of the seven instruments could be included in the comparison, values scattered by less than a factor of 3. Suspension methods and particle methods included in our study yielded similar average numbers of INM per particle/droplet, as can be seen by the fact that λ was found to be proportional to the particle volume and by the fact that n_m agreed well for the different instruments over the whole temperature range. Here it shows that it might have been advantageous, that the bacterial cells were torn apart in the atomizer which we used to produce particles. If we had dealt with whole bacterial cells, these cells could not have been distributed into particles smaller than the cell size, and λ would have dropped to 0 sharply for these small particles. It also is of advantage that Snomax contains much soluble material, as particles produced from solutions tend to be more spherical than e.g., insoluble mineral dust particles. As we found that the relation between suspension methods and particle methods could be based on a simple relation of the mass of Snomax to the volume of Snomax particles, particle shape can be assumed to have been close to sphericity. This facilitates the comparison of results from the different instruments. More difficulties might arise for less spherical INP or for substances where the relation between mass (or surface) of the INP and number of the ice-active entities is not as simple. We propose that Snomax indeed is a substance which can be used as a model sample when testing instrumentation

with respect to performance in immersion freezing, particularly in the temperature range where the strong increase in measured ice fractions is seen, but also at lower temperatures. For the latter, conditions of the experiment should be chosen such that not all droplets carry an INM, which can be reached by examining sub micron dry particles or sufficiently diluted suspensions, because this enables to measure frozen fractions below 1 and hence gain additional information about the performance of the instrument.

Two parameterizations taken from literature (Hartmann et al., 2013; Niedermeier et al., 2014) compared well with the data obtained in this study, although in these parameterizations the more ice-active INM had not been incorporated. Nevertheless, deviations over the whole course (from -2 to -38°C) are small enough to argue that these parameterizations, and also the time-independent parameterization based on Hartmann et al. (2013) derived in the present study (see Eq. 6) are applicable for describing immersion freezing induced by *P. syringae* bacteria over the whole temperature range in which immersion freezing occurs.

Appendix A: Instrumentation

A1 Acoustic levitator (AL)

The employed acoustic levitator is the type APOS BA 10 from the company TEC5. A standing ultrasonic wave is produced by interference between a radiator and a reflector. At the nodes drops can be levitated without any wall or substrate contact and without electrical charges (Diehl et al., 2009). For heterogeneous experiments the levitator is installed inside a walk-in cold chamber together with a platinum-resistor thermometer Pt100 to measure the ambient temperature. A digital video camera is used to record the freezing process and the droplet sizes. With an infrared thermometer the temperature of the freezing drops is measured directly and free of contact. As this requires a circular spot of approximately 1 mm in diameter, the investigated drops had sizes of 2.0 ± 0.1 mm in diameter (Diehl et al., 2014).

Because of their rather large volume and missing ventilated heat transfer, the levitated drops cooled down rather slowly while exchanging heat with the ambient air in the cold chamber which was approximately -23 °C during the Snomax experiments. This resulted in a non-linear cooling rate and the temperature of pure water drops in the levitator developed as follows (see also Fig. A1):

$$T_{\text{drop}}(t) = -21.83862 + 21.88997 \cdot \exp\left(-\frac{t}{15.3108}\right). \quad (\text{A1})$$

Individual drops containing Snomax in various concentrations were levitated one after another and cooled down according to Eq. (A1). The transition from the liquid to the ice phase was visible by a sudden increase of the droplet temperature (caused by the release of latent heat) recorded by the infrared thermometer. For each particle concentration, approximately 100 drops were observed until they froze and the freezing temperatures, i.e., the lowest droplet temperatures, were recorded with a measuring error of ± 0.7 K. Afterwards, for temperature steps of 1 K the fractions of frozen drops were counted.

A2 AIDA

The AIDA (Aerosol Interaction and Dynamics in the Atmosphere) controlled expansion cloud-simulation chamber (Möhler et al., 2003) was used to measure the droplet-freezing activity of Snomax particles during expansion cooling. The experimental procedure of AIDA immersion mode freezing measurements is described in previous literature (Hiranuma et al., 2014; Niemand et al., 2012) and is only briefly discussed here. The AIDA chamber consists of a thermally instated 84 m^3 aluminum vessel and an industrial air pump to simulate the adiabatic cooling of an updrafted air parcel by mechanical cooling. Due to the continuous cooling, water vapor becomes fully saturated inside the vessel, resulting in freezing of Snomax particles immersed in water

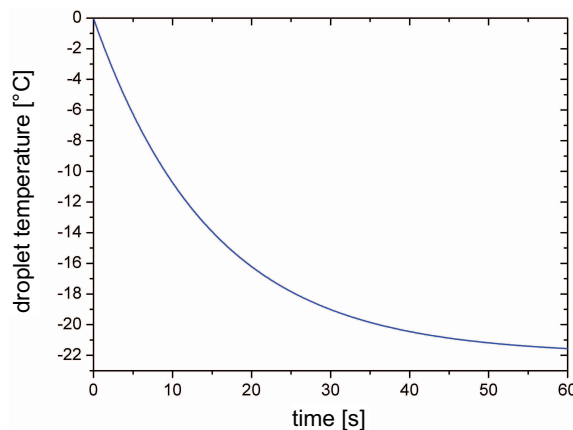


Figure A1. Development of droplet temperature during cooling in the AL.

droplets. Consequently, AIDA enables experiments with an abundant concentration of supercooled droplets (up to several hundred droplets per cubic centimeter) and atmospherically relevant supercooled droplet sizes (several micrometer in diameter) within experimental uncertainties in temperature of ± 0.3 K and in relative humidity with respect to water of ± 5 %.

The injection of Snomax particles into the AIDA chamber was carried out by atomization of a Snomax suspension (5 g Snomax in 1 L of $18.2 \text{ M}\Omega\text{cm}$ ultrapure water). For consistency with other INUIT project partners, the same atomizer type was used at AIDA for particle generation. Accordingly, aerosolized Snomax particles were directed into the ventilated AIDA vessel and characterized for number concentration (N_{ae}) and particle size distribution by a Scanning Mobility Particle Sizer (SMPS, TSI, Model 3080 DMA and Model 3010 condensation particle counter) and an Aerosol Particle Sizer (APS, TSI, Model 3321) prior to each expansion experiment.

During the typical AIDA expansion experiments carried out for the present work, a constant mechanical pumping created the chamber pressure drop from atmospheric pressure to roughly 900 mbar, resulting in time-averaged cooling rates of about 1 to 3 K min^{-1} . A total of nine expansions (three poly-disperse and six size-selected measurements) was performed and immersion freezing activities of Snomax aerosols were recorded in the temperature range from -7.5 to -11.5 °C. The number density of activated ice, N_{ice} , was measured by the Welas optical particle counter (PALAS, Sensor series 2300 and 2500, Benz et al., 2005) installed on the bottom of the vessel during each expansion, and was later on used to evaluate the activated ice fraction ($f_{\text{ice}} = N_{\text{ice}}/N_{\text{ae}}$). We note that four expansions were carried starting roughly at -9 °C, in order to estimate f_{ice} in the temperature region below -9 °C with a minimum influence of ice losses by the settling of ice crystals.

A3 BINARY

The BINARY (Bielefeld Ice Nucleation ARraY) setup consists of an array of 36 microliter-sized droplets positioned on a thin hydrophobic glass surface placed on a Peltier cooling stage (Budke and Koop, 2015). With the Peltier stage connected to a sink bath at 5 °C, the droplets can be cooled to −40 °C at cooling rates between 0.1 and 10 °C min^{−1}. Heterogeneous ice nucleation at the glass surface is minimized due to the hydrophobicity of the glass, and also by using freshly double-distilled water. The droplets are separated from each other by a polydimethylsiloxane (PDMS) spacer and the resulting compartments are sealed at the top with another glass slide. The droplet separation prevents a Wegener–Bergeron–Findeisen process, in which frozen droplets grow at the expense of unfrozen, i.e., supercooled liquid, droplets due to the vapor pressure difference between ice and supercooled liquid water (Murphy and Koop (2005)). During an experiment the droplet array is monitored continuously with a CCD camera which enables the automatic detection of nucleation events. A LabVIEW™ virtual instrument is used to control the temperature of the Peltier stage and to analyze in real time the obtained digital images, typically recorded every 6 s. Freezing is determined optically based on the change in brightness when the transparent liquid droplets become opaque upon freezing. The mean gray value, *gv*, (ranging from *gv* = 0 (black) to *gv* = 255 (white)) is determined for each compartment/droplet *i* in every image *j*, i.e., at every temperature. The difference in *gv* between successive images and, hence, temperatures $\Delta gv_{i,j} = gv_{i,j} - gv_{i,j-1}$ is then used to determine freezing and melting events. Typical gray value differences $\Delta gv_{i,j}$ upon freezing are larger than ~ 10 , while the maximum background noise value is well below ± 1 , which we set as the threshold value for freezing and melting, respectively.

A4 FINCH

FINCH (Fast Ice Nucleus CHamber) consists of an 80 cm long flow tube (8.8 cm inner diameter), which can be cooled down to −65 °C. Right before entering the tube on the top the sample flow is cooled and mixed with particle-free, humidified, warm air as well as with dry, cold air. The mixing of the different air flows and the cooling of the tube results in a defined freezing temperature and supersaturation inside the tube (Bundke et al., 2008). For the present study FINCH was operated at 150 % RH_i (relative humidity with respect to ice), which is well above water saturation for the used range of freezing temperatures. Therefore, particles that are entering the flow tube grow to droplets and subsequently freeze depending on the nature of the immersed aerosol particle and the adjusted freezing temperature. An optical detector similar to Bundke et al. (2010) is mounted at the outlet of the flow tube. It determines whether the arriving hydromete-

ors are liquid droplets or frozen ice crystals from which the frozen fraction *f*_{ice} can be calculated.

FINCH measurements were performed on size-segregated particles, which were produced by atomizing a Snomax suspension (1 g Snomax in 1 L of deionized water, using the same atomizer as for AIDA, LACIS, and PINC measurements). After spraying, the particles were dried in a silica diffusion drier and size-selected by a DMA (Differential Mobility Analyzer, TSI 3081, sheath flow of 3 L min^{−1}). The monodisperse aerosol flow (~ 0.1 to 0.3 L min^{−1}) was mixed with ~ 2.7 to 2.9 L min^{−1} of dry, particle-free air to reduce the number of particles considerably. For the measurements with FINCH a particle number concentration of less than ~ 1500 L^{−1} is aimed at to avoid particle coincidence in the detector.

A5 LACIS

LACIS (Leipzig Aerosol Cloud Interaction Simulator) was used in its immersion freezing mode (Hartmann et al., 2011) for the study presented here. LACIS is a 7 m long flow tube, consisting of 1 m sections which can be temperature controlled separately. Temperatures can go down to −40 °C. Before entering the flow tube, the sheath air stream is hydrated such – by use of a humidifier (PH-30T-24KS, Perma Pure) – that droplets form on the aerosol particles upon cooling, i.e., during the passage of the flow tube. These droplets can subsequently freeze, depending on the nature of the immersed aerosol particle and the adjusted temperature. At the LACIS outlet, a self-built optical particle spectrometer (TOPS-Ice, Clauss et al., 2013) determines if the arriving hydrometeors are liquid droplets or frozen ice crystals, resulting in the determination of a frozen fraction, *f*_{ice}.

LACIS measurements were performed on size-segregated particles which were produced by atomizing a Snomax suspension (5 g Snomax in 1 L of 18.2 MΩcm ultrapure water, using exactly the same atomizer as used for AIDA, FINCH and PINC measurements). After spraying, the particles were dried and size-selected by a DMA (Differential Mobility Analyzer, type Vienna Hauke medium, aerosol to sheath air flow ratio of 1 : 5) and provided for further analysis.

For a more detailed description of the particle generation and measurement procedure see Hartmann et al. (2013), where similar measurements were introduced, differing only in the use of a different batch of Snomax, the use of a different atomizer, and the use of a different concentration in the sprayed suspension (1.6 g L^{−1}), which, however, does not influence the particle generation as the aerosol was dried after spraying.

A6 Mainz vertical wind tunnel (WT)

In the Mainz vertical wind tunnel, drops are freely floated at their terminal velocities in an air stream. Thus, ventilation and heat transfer are similar to the situation in the real at-

mosphere. The wind speed is uniformly distributed around the tunnel cross section area up to the boundary layer at the tunnel walls. This ensures that drops float in a stable fashion in the experimental section of the tunnel (Diehl et al., 2011). The droplet sizes were calculated from the recorded wind speed in the tunnel as it must be equal to the terminal velocity of the droplet to keep the droplet floating in the experimental section. The droplet temperature was determined from the ambient temperature in the wind tunnel and the dew point with an estimated error of ± 0.75 K.

The experiments were performed in a manner very similar to earlier studies with pollen (Diehl et al., 2002; v. Blohn et al., 2005) at constant ambient temperatures; i.e., the wind tunnel was pre-cooled to certain temperatures in steps of 1 K. The adaption time of the drops, i.e., the time after which the droplet temperature was equal to the ambient temperature, was calculated according to Pruppacher and Klett (1997) (Chapt. 13) by considering ventilation and heat transfer of a droplet floating in an air stream. The results indicate that drops of the investigated sizes reached the ambient temperatures of -5 to -18 °C in the wind tunnel after 3 to 4 s. Individual drops of 760 μm diameter containing Snomax in two different concentrations were observed for approximately 30 to 40 s. Per temperature interval and Snomax concentration around 50 drops were investigated. The fractions of frozen drops were counted for a total observation time of 30 s.

A7 PINC

The Portable Ice Nucleation Chamber (PINC) operation principle is based on the Continuous Flow Diffusion Chamber (CFDC; Rogers, 1988) with two flat parallel plates (568×300 mm) whose inner walls are iced before each experiment. Applying a temperature gradient between the two iced walls leads to supersaturation with respect to ice and water and allows ice crystals to form and grow on ice nuclei in the sub-saturated ($\text{RH} < 100\%$) and supersaturated ($\text{RH} > 100\%$) regimes. For conditions when ice nucleation is observed at $\text{RH}_w < 100\%$, deposition mode ice formation is inferred, whereas for any ice formation observed at $\text{RH}_w > 100\%$, condensation/immersion freezing is implied. Droplets evaporate in the evaporation section downstream of the freezing chamber. Upstream of PINC, aerosol particles are counted with a condensation particle counter (CPC) after flowing through an impactor with a D50 cutoff at 0.91 μm aerodynamic diameter (Chou et al., 2011). The ice crystals are counted with an optical particle counter (OPC) at the exit of PINC and are distinguished from the small unactivated aerosol particles by their size.

Further details on the PINC design are described in Chou et al. (2011) and Kanji et al. (2013). The activated fraction is calculated by taking the ratio of the ice crystal number concentration to the total particle number concentration measured with the CPC. For comparison with other ice nucleation counters measuring in the immersion mode, only data

taken by PINC at $\text{RH}_w \geq 100\%$ and below the RH_w at which droplets survive past the evaporation section (RH_{w,d_s}), are presented. For each temperature, RH was scanned continuously from $\text{RH}_i = 100\%$ up to RH_{w,d_s} . At $T = -20$ °C, RH_{w,d_s} is 104.5%. However, at $T = -10$ °C it decreases to 101.7%. Particle losses in the tubing and the impactor upstream of PINC were accounted for by a particle loss curve which was found for kaolinite particles with a mobility diameter between 500–950 nm or measured before the experiment using Snomax (for measurements at $T > -12$ °C).

Temperature uncertainties in PINC are on the order of ± 0.1 K resulting in a relative uncertainty of $\pm 2\%$ in relative humidity. The temperature uncertainty results in a variation across the sample lamina of up to 0.8 K (± 0.4 K). The uncertainty in n_m from the optical particle counter is 10%.

Measurements were made during three different occasions. Measurements were done in Leipzig in parallel to LACIS measurements (data labeled with #1), where particles were produced using the INUIT Snomax batch and the atomizer used within the INUIT community. During these measurements, PINC only measured at $T < -14$ °C, due to instrumental issues during the campaign. Snomax from the INUIT batch was then also used for measurements at ETH, and care had been taken to store the sample frozen at all times (stored at -18.2 °C). The respective data are labeled #2. At ETH, also Snomax from a different batch was used, and the respective data are marked by #3 (this Snomax sample was stored at $+5$ °C). PINC measurements done at ETH, including all measurements at $T > -12$ °C, were performed with Snomax particles prepared by suspending 0.08 g or 0.4 g Snomax in 80 mL of deionized distilled water (DDW, 18.2 M Ωcm) (#2 and #3, respectively). Particles were suspended using an atomizer and size-selected at 500 nm with a DMA (TSI, 1 : 5 sample to sheath air ratio).

The results suggest a good agreement between LACIS and PINC data at temperatures below -14 °C. At warmer temperatures, a RH_w of 100 to 101.7% and the short residence time of the aerosol particles in PINC of 5 s might not be sufficient to guarantee droplet formation. Thus, it is possible that we do not observe immersion freezing at these conditions, but rather deposition or condensation nucleation of ice.

Acknowledgements. The present study was done within the DFG funded Ice Nucleation research UnIT (INUIT, FOR 1525), including project BU 1432/4-1, DI 1539/1-1, KO 2944/2-1, MO 668/4-1, and WE 4722/1-1. Z. A. Kanji and Y. Boose would like to acknowledge SNF for funding. The authors also thank the two referees of this work, Russel Schnell and Gabor Vali, for their encouraging reviews.

Edited by: A. Bertram

References

- Ansmann, A., Tesche, M., Seifert, P., Althausen, D., Engelmann, R., Fruntke, J., Wandinger, U., Mattis, I., and Müller, D.: Evolution of the ice phase in tropical altocumulus: SAMUM lidar observations over Cape Verde, *J. Geophys. Res.*, 114, D17208, doi:10.1029/2008JD011659, 2009.
- Atkinson, J. D., Murray, B. J., Woodhouse, M. T., Whale, T. F., Baustian, K. J., Carslaw, K. S., Dobbie, S., O'Sullivan, D., and Malkin, T. L.: The importance of feldspar for ice nucleation by mineral dust in mixed-phase clouds, *Nature*, 498, 355–358, doi:10.1038/nature12278, 2013.
- Attard, E., Yang, H., Delort, A.-M., Amato, P., Pöschl, U., Glaux, C., Koop, T., and Morris, C. E.: Effects of atmospheric conditions on ice nucleation activity of *Pseudomonas*, *Atmos. Chem. Phys.*, 12, 10667–10677, doi:10.5194/acp-12-10667-2012, 2012.
- Augustin, S., Wex, H., Niedermeier, D., Pummer, B., Grothe, H., Hartmann, S., Tomsche, L., Clauss, T., Voigtländer, J., Ignatius, K., and Stratmann, F.: Immersion freezing of birch pollen washing water, *Atmos. Chem. Phys.*, 13, 10989–11003, doi:10.5194/acp-13-10989-2013, 2013.
- Benz, S., Megahed, K., Möhler, O., Saathoff, H., Wagner, R., and Schurath, U.: T-dependent rate measurements of homogeneous ice nucleation in cloud droplets using a large atmospheric simulation chamber, *J. Photochem. Photobiol.*, 176, 208–217, 2005.
- Budke, C. and Koop, T.: BINARY: an optical freezing array for assessing temperature and time dependence of heterogeneous ice nucleation, *Atmos. Meas. Tech.*, 8, 689–703, doi:10.5194/amt-8-689-2015, 2015.
- Bühl, J., Ansmann, A., Seifert, P., Baars, H., and Engelmann, R.: Toward a quantitative characterization of heterogeneous ice formation with lidar/radar: comparison of CALIPSO/CloudSat with ground-based observations, *Geophys. Res. Lett.*, 40, 4404–4408, doi:10.1002/grl.50792, 2013.
- Bundke, U., Nillius, B., Jaenicke, R., Wetter, T., Klein, H., and Bingemer, H.: The fast Ice Nucleus chamber FINCH, *Atmos. Res.*, 90, 180–186, doi:10.1016/j.atmosres.2008.02.008, 2008.
- Bundke, U., Reimann, B., Nillius, B., Jaenicke, R., and Bingemer, H.: Development of a Bioaerosol single particle detector (BIO IN) for the Fast Ice Nucleus CHamber FINCH, *Atmos. Meas. Tech.*, 3, 263–271, doi:10.5194/amt-3-263-2010, 2010.
- Chou, C., Stetzer, O., Weingartner, E., Jurányi, Z., Kanji, Z. A., and Lohmann, U.: Ice nuclei properties within a Saharan dust event at the Jungfraujoch in the Swiss Alps, *Atmos. Chem. Phys.*, 11, 4725–4738, doi:10.5194/acp-11-4725-2011, 2011.
- Clauss, T., Kiselev, A., Hartmann, S., Augustin, S., Pfeifer, S., Niedermeier, D., Wex, H., and Stratmann, F.: Application of linear polarized light for the discrimination of frozen and liquid droplets in ice nucleation experiments, *Atmos. Meas. Tech.*, 6, 1041–1052, doi:10.5194/amt-6-1041-2013, 2013.
- Cochet, N. and Widehem, P.: Ice crystallization by *Pseudomonas syringae*, *Appl. Microbiol. Biot.*, 54, 153–161, 2000.
- Conen, F., Morris, C. E., Leifeld, J., Yakutin, M. V., and Alewell, C.: Biological residues define the ice nucleation properties of soil dust, *Atmos. Chem. Phys.*, 11, 9643–9648, doi:10.5194/acp-11-9643-2011, 2011.
- Cziczo, D. J., Froyd, K. D., Hoose, C., Jensen, E. J., Diao, M., Zondlo, M. A., Smith, J. B., Twohy, C. H., and Murphy, D. M.: Clarifying the dominant sources and mechanisms of cirrus cloud formation, *Science*, 340, 1320–1324, doi:10.1126/science.1234145, 2013.
- DeMott, P. J., Möhler, O., Stetzer, O., Vali, G., Levin, Z., Peters, M. D., Murakami, M., Leisner, T., Bundke, U., Klein, H., Kanji, Z. A., Cotton, R., Jones, H., Benz, S., Brinkmann, M., Rzesanke, D., Saathoff, H., Nicolet, M., Saito, A., Nillius, B., Bingemer, H., Abbatt, J., Ardon, K., Ganor, E., Georgakopoulos, D. G., and Saunders, C.: Resurgence in ice nuclei measurement research, *B. Am. Meteorol. Soc.*, 92, 1623–1635, doi:10.1126/science.1234145, 2011.
- Diehl, K., Matthias-Maser, S., Mitra, S. K., and Jaenicke, R.: The ice nucleating ability of pollen. Part II: Laboratory studies in immersion and contact freezing modes, *Atmos. Res.*, 61, 125–133, 2002.
- Diehl, K., Ettner-Mahl, M., Hannemann, A., and Mitra, S. K.: Homogeneous freezing of single sulfuric and nitric acid solution drops levitated in an acoustic trap, *Atmos. Res.*, 94, 356–361, 2009.
- Diehl, K., Mitra, S. K., Szakáll, M., v. Blohn, N., Borrmann, S., and Pruppacher, H. R.: The Mainz vertical wind tunnel facility: a review of 25 years of laboratory experiments on cloud physics and chemistry, in: *Wind Tunnels: Aerodynamics, Models, and Experiments.*, edited by: Pereira, J., Nova Science Publishers Inc., Hauppauge, NY, Chapter 2, 2011.
- Diehl, K., Debertshäuser, M., Eppers, O., Schmithüsen, H., Mitra, S. K., and Borrmann, S.: Particle surface area dependence of mineral dust in immersion freezing mode: investigations with freely suspended drops in an acoustic levitator and a vertical wind tunnel, *Atmos. Chem. Phys.*, 14, 12343–12355, doi:10.5194/acp-14-12343-2014, 2014.
- Fröhlich-Nowoisky, J., Hill, T. C. J., Pummer, B. G., Franc, G. D., and Pöschl, U.: Ice Nucleation Activity in the Widespread Soil Fungus *Mortierella alpina*, *Biogeosciences Discuss.*, 11, 12697–12731, doi:10.5194/bgd-11-12697-2014, 2014.
- Garnham, C. P., Campbell, R. L., Walker, V. K., and Davies, P. L.: Novel dimeric beta-helical model of an ice nucleation protein with bridged active sites, *BMC Struct. Biol.*, 11, doi:10.1186/1472-6807-11-36, 2011.
- Govindarajan, A. G. and Lindow, S. E.: Size of bacterial ice-nucleation sites measured in situ by radiation inactivation analysis, *P. Natl. Acad. Sci. USA*, 85, 1334–1338, doi:10.1073/pnas.85.5.1334, 1988.
- Green, R. L. and Warren, G. J.: Physical and functional repetition in a bacterial ice nucleation gene, *Nature*, 317, 645–648, doi:10.1038/317645a0, 1985.
- Hallett, J. and Mossop, S. C.: Production of secondary ice particles during the riming process, *Nature*, 249, 26–28, doi:10.1038/249026a0, 1974.
- Hartmann, S., Niedermeier, D., Voigtländer, J., Clauss, T., Shaw, R. A., Wex, H., Kiselev, A., and Stratmann, F.: Homogeneous and heterogeneous ice nucleation at LACIS: operating principle and theoretical studies, *Atmos. Chem. Phys.*, 11, 1753–1767, doi:10.5194/acp-11-1753-2011, 2011.
- Hartmann, S., Augustin, S., Clauss, T., Wex, H., Šantl-Temkiv, T., Voigtländer, J., Niedermeier, D., and Stratmann, F.: Immersion freezing of ice nucleation active protein complexes, *Atmos. Chem. Phys.*, 13, 5751–5766, doi:10.5194/acp-13-5751-2013, 2013.

- Hasegawa, Y., Ishihara, Y., and Tokuyama, T.: Characteristics of ice nucleation in *Fusarium avenaceum* IFO 7158, Biosci. Biotech. Bioch., 58, 2273–2274, 1994.
- Hiranuma, N., Hoffmann, N., Kiselev, A., Dreyer, A., Zhang, K., Kulkarni, G., Koop, T., and Möhler, O.: Influence of surface morphology on the immersion mode ice nucleation efficiency of hematite particles, Atmos. Chem. Phys., 14, 2315–2324, doi:10.5194/acp-14-2315-2014, 2014.
- Kanji, Z. A., Welti, A., Chou, C., Stetzer, O., and Lohmann, U.: Laboratory studies of immersion and deposition mode ice nucleation of ozone aged mineral dust particles, Atmos. Chem. Phys., 13, 9097–9118, doi:10.5194/acp-13-9097-2013, 2013.
- Koop, T. and Zobrist, B.: Parameterizations for ice nucleation in biological and atmospheric systems, Phys. Chem. Chem. Phys., 11, 10839–10850, 2009.
- Maki, L. R., Galyan, E. L., Changchi, M.-M., and Caldwell, D. R.: Ice nucleation induced by *Pseudomonas syringae*, Appl. Microbiol., 28, 456–459, 1974.
- McMurry, P. H., Wang, X., Park, K., and Ehara, K.: The relationship between mass and mobility for atmospheric particles: a new technique for measuring particle density, Aerosol Sci. Tech., 36, 227–238, 2002.
- Möhler, O., Stetzer, O., Schaefers, S., Linke, C., Schnaiter, M., Tiede, R., Saathoff, H., Krämer, M., Mangold, A., Budz, P., Zink, P., Schreiner, J., Mauersberger, K., Haag, W., Kärcher, B., and Schurath, U.: Experimental investigation of homogeneous freezing of sulphuric acid particles in the aerosol chamber AIDA, Atmos. Chem. Phys., 3, 211–223, doi:10.5194/acp-3-211-2003, 2003.
- Möhler, O., Georgakopoulos, D. G., Morris, C. E., Benz, S., Ebert, V., Hunsmann, S., Saathoff, H., Schnaiter, M., and Wagner, R.: Heterogeneous ice nucleation activity of bacteria: new laboratory experiments at simulated cloud conditions, Biogeosciences, 5, 1425–1435, doi:10.5194/bg-5-1425-2008, 2008.
- Morris, C. E., Georgakopoulos, D. G., and Sands, D. C.: Ice nucleation active bacteria and their potential role in precipitation, J. Phys. IV, 121, 87–103, doi:10.1051/jp4:2004121004, 2004.
- Murphy, D. M. and Koop, T.: Review of the vapour pressures of ice and supercooled water for atmospheric applications, Q. J. Roy. Meteor. Soc., 131, 1539–1565, 2005.
- Murray, B. J., O’Sullivan, D., Atkinson, J. D., and Webb, M. E.: Ice nucleation by particles immersed in supercooled cloud droplets, Chem. Soc. Rev., 41, 6519–6554, 2012.
- Niedermeier, D., Ervens, B., Clauss, T., Voigtländer, J., Wex, H., Hartmann, S., and Stratmann, F.: A computationally efficient description of heterogeneous freezing: a simplified version of the Soccer ball model, Geophys. Res. Lett., 41, 736–741, doi:10.1002/2013GL058684, 2014.
- Niemand, M., Möhler, O., Vogel, B., Vogel, H., Hoose, C., Connolly, P., Klein, H., Bingemer, H., DeMott, P., Skrotzki, J., and Leisner, T.: A particle-surface-area-based parameterization of immersion freezing on desert dust particles, J. Atmos. Sci., 69, 3077–3092, doi:10.1175/jas-d-11-0249.1, 2012.
- Orser, C., Staskawicz, B. J., Panopoulos, N. J., Dahlbeck, D., and Lindow, S. E.: Cloning and expression of bacterial ice nucleation genes in *Escherichia-Coli*, J. Bacteriol., 164, 359–366, 1985.
- O’Sullivan, D., Murray, B. J., Malkin, T. L., Whale, T. F., Umo, N. S., Atkinson, J. D., Price, H. C., Baustian, K. J., Browse, J., and Webb, M. E.: Ice nucleation by fertile soil dusts: relative importance of mineral and biogenic components, Atmos. Chem. Phys., 14, 1853–1867, doi:10.5194/acp-14-1853-2014, 2014.
- Pruppacher, H. R. and Klett, J. D.: Microphysics of Clouds and Precipitation, Kluwer Academic Publishers, Dordrecht, the Netherlands, Chapter 13, 1997.
- Pummer, B. G., Bauer, H., Bernardi, J., Bleicher, S., and Grothe, H.: Suspendable macromolecules are responsible for ice nucleation activity of birch and conifer pollen, Atmos. Chem. Phys., 12, 2541–2550, doi:10.5194/acp-12-2541-2012, 2012.
- Rogers, D. C.: Development of a continuous flow thermal gradient diffusion chamber for ice nucleation studies, Atmos. Res., 22, 149–181, 1988.
- Schnell, R. and Vali, G.: Biogenic ice nuclei: Part I. Terrestrial and marine sources, J. Atmos. Sci., 33, 1554–1564, 1976.
- Southworth, M. W., Wolber, P. K., and Warren, G. J.: Nonlinear relationship between concentration and activity of a bacterial ice nucleation protein, J. Biol. Chem., 263, 15211–15216, 1988.
- Szyrmer, W. and Zawadzki, I.: Biogenic and anthropogenic sources of ice-forming nuclei: a review, B. Am. Meteorol. Soc., 78, 209–228, 1997.
- Tobo, Y., DeMott, P. J., Hill, T. C. J., Prenni, A. J., Swoboda-Colberg, N. G., Franc, G. D., and Kreidenweis, S. M.: Organic matter matters for ice nuclei of agricultural soil origin, Atmos. Chem. Phys., 14, 8521–8531, doi:10.5194/acp-14-8521-2014, 2014.
- Turner, M. A., Arellano, F., and Kozloff, L. M.: Three separate classes of bacterial ice nucleation structures, J. Bacteriol., 172, 2521–2526, 1990.
- Ukhatskaya, E. V., Kurkov, S. V., Matthews, S. E., and Loftsson, T.: Antifungal drug solubilizing activity and self-aggregation ability of cationic aminocalix[4]arene in comparison to SBE β CD: effect of addition of water-soluble polymer, J. Incl. Phenom. Macro., 79, 47–55, doi:10.1007/s10847-013-0302-5, 2014.
- v. Blohn, N., Mitra, S. K., Diehl, K., and Borrmann, S.: The ice nucleating ability of pollen. Part III: New laboratory studies in immersion and contact freezing modes including more pollen types, Atmos. Res., 78, 182–189, doi:10.1016/j.atmosres.2005.03.008, 2005.
- Vali, G.: Quantitative evaluation of experimental results on heterogeneous freezing nucleation of supercooled liquids, J. Atmos. Sci., 28, 402–409, 1971.
- Wolber, P. K., Deininger, C. A., Southworth, M. W., Vandekerckhove, J., Vanmontagu, M., and Warren, G. J.: Identification and purification of a bacterial ice-nucleation protein, P. Natl. Acad. Sci. USA, 83, 7256–7260, 1986.
- Wood, S. E., Baker, M. B., and Swanson, B. D.: Instrument for studies of homogeneous and heterogeneous ice nucleation in free-falling supercooled water droplets, Rev. Sci. Instrum., 73, 3988–3996, 2002.
- Yankofsky, S. A., Levin, Z., Bertold, T., and Sandlerman, N.: Some basic characteristics of bacterial freezing nuclei, J. Appl. Meteorol., 20, 1013–1019, 1981.